International Journal of Hydrogen Energy xxx (xxxx) xxx

Contents lists available at ScienceDirect

International Journal of Hydrogen Energy

journal homepage: www.elsevier.com/locate/he

Assessing PEM fuel cell performance in a geothermal Cogeneration system for peak-time energy storage

Ehsanolah Assareh [a,b,c,1,**], Salah Noori Ali [d,1], Parviz Ghafariasl [e,1], Siamak Hoseinzadeh [f,1,*], Neha Agarwal [b,1], Moonyong Lee [b,***], Davide Astiaso Garcia [f]

[a] Department of Renewable Energy Technology, Materials and Energy Research Center, Dezful Branch, Islamic Azad University, Dezful, Iran
[b] School of Chemical Engineering, Yeungnam University, Gyeongsan, 38541, South Korea
[c] Built Environment and Engineering Program, College of Sport, Health and Engineering (CoSHE), Victoria University, Melbourne, Australia
[d] Department of Mechanical Engineering, Science and Research Branch, Islamic Azad University, Tehran, Iran
[e] Department of Industrial and Manufacturing Systems Engineering, Kansas State University, Manhattan, KS, USA
[f] Department of Planning, Design, Technology of Architecture, Sapienza University of Rome, Via Flaminia 72, 00196, Rome, Italy

ARTICLE INFO

Handling Editor: Ibrahim Dincer

Keywords:
Geothermal energy
Absorption chiller
PEMFC
Organic rankine cycle (ORC)
EPEM

ABSTRACT

In this investigation, a novel geothermal power plant was designed, combining absorption chiller units, PEMFC, EPEM, and ORC. We conducted a comprehensive case study across four continents—Asia, Oceania, Europe, and America—leveraging weather data from various cities to evaluate the system's efficacy. Our modeling utilized EES (Engineering Equation Solver) software, optimizing the setup via the RSM with three key objective functions: exergy efficiency, hydrogen production, and cost rate. The primary focus was on delivering electricity to residential properties during peak demand periods. Exploring six scenarios for organic fluids in organic Rankine cycles, we gauged energy, exergy, and overall system performance. The TOPSIS method led us to select scenario 3, employing R123 and R134a refrigerants, as the optimal choice. The results of the optimization showcased impressive figures: an exergy efficiency of 81.816%, a hydrogen production rate of 25.119 kg/h, and a cost rate of 15.967 $/h for the system's most efficient configuration. Economic analysis highlighted the organic Rankine cycle units 1 and 2 as the components with the highest costs. Our evaluation extended to various cities—Aomori, Grosseto, Lhasa, Wellington, and San Diego—assessing the electricity, heating, and cooling needs of residential complexes based on the system's performance.

Nomenclature

T_0	Ambient temperature [°C]	n	Period of performance
$\dot{Z}$	Cost rate [$/h]	**Abbreviations**	
$\dot{Ex}$	Exergy [kW]	ORC	Organic Rankine Cycle
T	Temperature [°C]	tur	Turbine
$\dot{m}$	Mass flow rate [kg/s]	cond	Condenser
s	Specific entropy [kJ/kg.K]	CRF	Capital Recover Factor

(*continued on next column*)

(*continued*)

$\dot{Q}$	Heat transfer rate [kW]	*eva*	Evaporator
x	Salinity [ppm]	PEMFC	Proton Exchange Membrane Fuel Cell
P_0	Ambient pressure [kPa]	HEX	Heat exchanger
h	Specific enthalpy [kj/kg]	FC	Fuel Cell
m	Mass Rate	EPEM	Electrolysis of proton exchange membrane
W	Power [kW]	**Greek symbol**	

(*continued on next page*)

* Corresponding author.
** Corresponding author.
*** Corresponding author.
E-mail addresses: Ehsanolah.assareh@gmail.com, Ehsanolah.assareh@yu.ac.kr, Ehsanolah.assareh@vu.edu.au (E. Assareh), siamak.hosseinzadeh@uniroma1.it, hoseinzadeh.siamak@gmail.com (S. Hoseinzadeh), mynlee@ynu.ac.kr (M. Lee).
[1] These authors contributed equally to this article as the first authors.

https://doi.org/10.1016/j.ijhydene.2024.08.080
Received 10 February 2024; Received in revised form 18 July 2024; Accepted 5 August 2024

(*continued*)

$\dot{E}x_D$	Exergy destruction	η	Efficiency
Subscripts		φ	Maintenance factor
pp	Pinch Point		
cv	Control Volume		
Ex	Exergy		

1. Introduction

The rising global population and the pursuit of better living standards have underscored the need for renewable power facilities, especially those tapping into abundant energy sources like geothermal, to fulfill the energy needs of residential structures. Furthermore, these endeavors directly address urgent environmental concerns [1]. Renewable energies, such as geothermal potential, play a critical role in alleviating the impacts of climate change and the rise in global temperatures [2]. Geothermal energy, derived from the Earth's internal heat interacting with subterranean water reservoirs, stands distinct as a renewable energy source unaffected by solar influences [3–5].

Rankine cycles serve as widely used power generation systems across the globe. The utilization of organic Rankine cycles, employing diverse working fluids, offers an avenue to boost the effectiveness of Rankine cycles [6,7]. This innovation, centered on organic Rankine cycles, taps into geothermal energy to produce electricity, presenting a clean energy alternative free from pollution [8–10]. Incorporating fuel cells reliant on hydrogen fuel can further enhance system power generation and facilitate better management of energy demands, contributing significantly to environmental conservation [11,12]. To optimize energy efficiency and cost-effectiveness, several strategies are advised, including the recovery of waste heat for additional electricity generation, simultaneous operation of multiple cycles [13], direct utilization of heat to power absorption chillers for cooling purposes [14], and fulfilling the electricity needs of the electrolyzer system [15]. These strategies collectively bolster the sustainability and performance of geothermal-based power generation setups.

In Cao et al.'s (2018) investigation, a geothermal system was explored, integrating the Kalina cycle, absorption refrigeration cycle, and an electrolyzer to enable ice production and hydrogen generation. Their findings unveiled a novel system boasting an impressive exergy efficiency reaching 23.59% [16].

Alirahmi and Assareh (2020) proposed a geothermal system to produce the required energy of a residential area in Iran and optimized the performance of the system for production with optimization methods [17].

Rin et al. (2019) introduced a renewable solar-geothermal system engineered for cooling, heating, and electricity generation. They applied a genetic algorithm with non-dominant sorting to optimize their proposed system. Their results underscored superior system performance when harnessing both solar and geothermal energies simultaneously, surpassing systems relying solely on a single renewable energy source [18].

Riolaa et al. (2019) proposed a distinctive geothermal-biomass power plant configuration, designed for regions facing water scarcity. This setup employed air-cooled condensers to address environmental constraints [19].

Li et al. (2020) presented a system integrated with a fuel cell unit, utilizing hot exhaust gases from biomass burning to generate electrical. Their study demonstrated impressive energy efficiency (67.3%) and exergy efficiency (29.2%), accompanied by a notable 13.9% reduction in carbon dioxide emissions [20].

Atiz et al. (2019) introduced a system leveraging a blend of geothermal and solar resources to enhance overall efficiency. Investigating diverse geothermal temperatures and organic fluids, they achieved substantial energy (6.92%) and exergy (21.06%) efficiencies. Notably, employing n-butane at an 86 °C geothermal source temperature showcased optimal performance [21].

Xie and Wang (2022) introduced geothermal-based electricity generation systems using various configurations, concluding that the single-flash system coupled with an ORC exhibited superior performance [22].

Zhong et al. (2022) conducted a feasibility assessment for clean electricity generation from an advanced geothermal system using vertical wells. Their study indicated promising potential for electricity output and efficiency [23].

Mardan Dezfouli et al. (2023) explored an optimal geothermal-based electricity generation system, revealing significant parameters such as output power, exergy destruction, and system efficiency [24].

Seiiedhoseiny et al. (2022) introduced a multifaceted geothermal system producing electricity and hydrogen. They noted trade-offs between cooling, heating, and electricity production based on varying flash tank pressures [25].

Pan et al. (2023) presented four geothermal systems utilizing liquefied natural gas's cold energy for electricity generation. Their research highlighted the substantial influence of separator pressure, and Rankine turbine inlet pressure on system performance [26].

Jiansheng et al. (2022) introduced an innovative geothermal system employing horizontal wells tailored for power generation. This system integrated an ORC unit, utilizing the organic fluid R245fa to bolster efficiency. Their findings underscored the significant impact of geothermal fluid mass flow rate on electricity production [27].

In today's world, energy stands as a pivotal concern, serving as the lifeblood of society. It's crucial to prudently manage current energy sources, safeguard fossil fuels for future generations, and transition towards clean, renewable energies to combat environmental pollution. Fossil fuel extraction and utilization have deeply affected multiple aspects of human life, spanning science, technology, economics, health, and the environment. The irreversible depletion of non-renewable energies presents a global challenge, and as fossil fuel combustion remains a primary source of environmental harm, exploring viable alternatives, notably renewable energy, is imperative.

Geothermal energy has gained prominence as a sustainable energy source, leveraging the earth's thermal energy for clean and sustainable electricity production. These systems hold particular relevance for residential areas situated in geothermally abundant regions.

The ongoing research aims to harness geothermal energy for generating vital resources like clean electricity and hydrogen, a well-known clean and carbon-free fuel. The primary objective is to curtail environmental pollution and establish crucial energy resources independent of fossil fuels.

The current research encompasses several pivotal components.

1. Introduction of an integrated geothermal system, incorporating a dual ORC, absorption chiller, (PEMFC, and Electrolyzer to optimize power, hydrogen, and cooling production.
2. Utilization of Grossman exergy diagrams to evaluate the system's efficiency.
3. Assessment of the geothermal power plant's viability across diverse regional climates.
4. Validation of the system's capability to fulfill the energy needs of residential structures.
5. Environmental impact analysis to gauge the ecological footprint of the proposed system.

The primary innovation lies in generating clean electrical energy using the multifunctional geothermal system, particularly during peak electricity demand periods. The system is engineered to address escalating energy needs during high-consumption periods. By integrating a hydrogen-powered fuel cell unit, the system bolsters its stability and reliability. In instances of reduced geothermal system stability, the fuel cell taps into stored hydrogen to supplement power, providing essential backup support.

A significant advantage is the utilization of hydrogen fuel, known for its efficiency and minimal environmental impact, rendering the system

clean and eco-friendly. Surplus electrical energy during low-demand periods can be fed back into the grid, contributing to cost mitigation. This research aims to tackle the challenges associated with peak energy demand in urban landscapes.

2. System introduction

That's a comprehensive system! Here's a more succinct representation:

The schematic of multiple study production system is shown in Fig. 1. This setup integrates a geothermal well, dual ORC units, an absorption chiller, a PEMFC, and an EPEM. The operational sequence involves.

1. Geothermal water from the well heats the evaporator, increasing the first ORC's temperature. The organic fluid in ORC 1 undergoes a cycle, transitioning from liquid to vapor in the evaporator, powering the turbine. The steam then heats the second ORC's working fluid via a heat exchanger before returning to a liquid state for recirculation.
2. ORC No. 2 operates similarly to ORC No. 1, using ambient air for cooling in its condenser. Both ORCs utilize refrigerant and ammonia as their working fluids.
3. Remaining geothermal water, still hot after ORC No. 1, is used in a single-effect absorption chiller to produce additional cooling by extracting its heat.
4. As the water system continues to operate, the cooled geothermal energy is returned to the earth to complete the cycle.
5. A PEMFC generates clean electricity using hydrogen produced by the EPEM unit. This fuel cell operates akin to a battery, continuously generating power when fueled by hydrogen and air.

Employing the PEMFC unit during peak demand, especially in high-

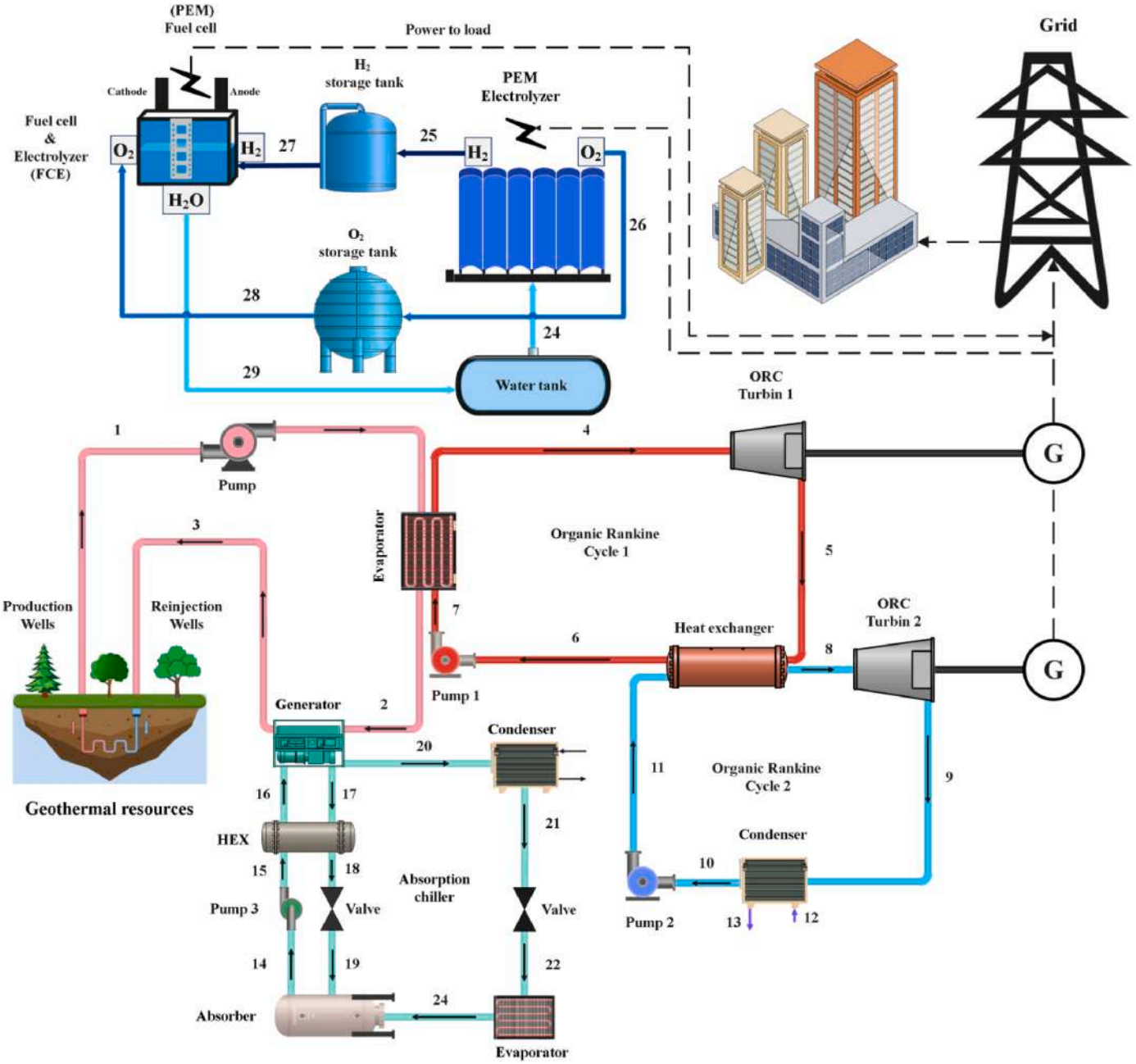

Fig. 1. Schematic of the system.

demand seasons like summer, serves as an effective strategy for meeting energy needs. This integrated system presents an innovative approach to leverage geothermal energy for power, hydrogen production, and cooling, supplemented by an efficient hydrogen fuel cell to ensure energy stability.

3. Methodology

Fig. 2 provides an overview of the methodology flowchart, outlining the step-by-step process as follows.

1. **System Modeling**: The modeling of the system is carried out using EES software. This involves setting up a detailed model of the proposed geothermal multi-production system.
2. **Selection of Organic Fluids**: To enhance the efficiency of the Rankine cycles, the most suitable organic fluids are selected. The TOPSIS method is employed for this purpose.
3. **Multi-Objective Optimization**: The system's overall performance is optimized by considering two objective functions. The optimization process is conducted using the Response Surface Method in conjunction with Design Expert software.
4. **Behavior Estimation and Prediction**: This stage involves estimating and predicting the behavior of the two objective functions in the optimized system.
5. **Weather Data Collection**: Weather information specific to the study city is obtained using Meteonorm software. This data is crucial for assessing the system's performance and feasibility in the respective climatic conditions.
6. **System Performance and Feasibility Check**: The system's performance is rigorously assessed, taking into account the specific climatic conditions of the studied cities. This step ensures that the proposed geothermal system can effectively operate in a range of climates.
7. **Energy Supply Evaluation**: The final phase involves investigating the system's capacity to supply energy to residential units throughout the year. This comprehensive evaluation assesses its ability to meet the energy needs of these units under varying conditions.

The entire methodology is designed to ensure the efficient operation and reliability of the suggested geothermal multi-production system, considering both technical and economic aspects, while adapting to diverse climatic conditions.

4. Modeling section

4.1. Thermodynamic analysis

In the modeling and analysis of the system, several key assumptions were made, as outlined in Refs. [28,29]. These assumptions include:

Omission of Pressure Losses: The calculation of pressure losses within the equipment was neglected. This simplification assumes that pressure losses within the system components are negligible.

Omission of Potential and Kinetic Energy Calculations: The calculations did not account for potential and kinetic energy within the system. It is assumed that the effects of potential and kinetic energy changes are not significant.

Steady-State Operation: The system is assumed to operate in a steady-state mode, implying that there are no significant transient or dynamic variations in the system's parameters.

To perform the thermodynamic analysis of the system, fundamental thermodynamic relationships were applied. These relationships are summarized in Table 1 and serve as the primary basis for the system's analysis [30,31].

Fixed data for geothermal system analysis are introduced in Table 2.

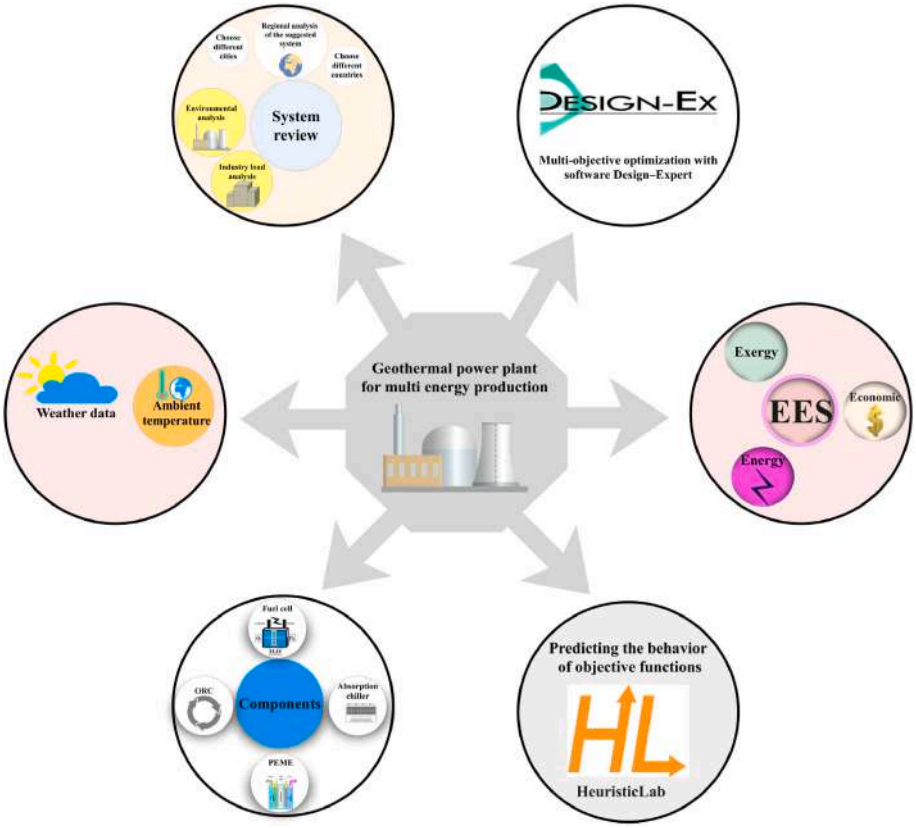

Fig. 2. Flowchart of problem solving.

Table 1
Thermodynamic analysis.

Basic relationships	Relation
Law of Survival of Crime	$\sum_k \dot{m}_i - \sum_k \dot{m}_e = \frac{dm_{cv}}{dt}$
Law of conservation of energy	$\dot{Q} - \dot{W} + \sum_i \dot{m}_i \left(h_i + \frac{v_i^2}{2} + gZ_i\right) - \sum_e \dot{m}_e \left(h_e + \frac{v_e^2}{2} + gZ_e\right) = \frac{dE_{cv}}{dt}$
Exergy balance	$\dot{E}x_Q + \sum_i \dot{m}_i(ex_i) = \sum_e \dot{m}_e(ex_e) + \dot{E}x_w + \dot{E}x_D$
Physical exergy	$\dot{E}x_{ph} = \sum_i \dot{m}_i((h_i - h_0) - T_0(s_i - s_0))$
Cost rate	$\dot{Z} = \frac{Z \times CRF \times \varphi}{T}$
Capital recovery factor	$CRF = \frac{k(1+k)^n}{(1+k)^n - 1}$

Table 2
Input data amount.

Parameter	Parameter introduction	Value
T_0	*Ambient temperature*	*25°C*
T_1	*Temperature of the Geothermal*	*180°C*
T_4	*Inlet temperature to turbine NO. 1*	*120°C*
P_0	*Ambient pressure*	*101.3* kPa
$\dot{m}_1$	*Mass flow rate of the Geothermal*	15 kg/s
pp_{Cond}	*Condenser of Pinch Point*	*5°C*
T_6	*Inlet temperature to pump NO. 1*	*40°C*
pp_{Eva}	*Evaporator of Pinch Point*	*5°C*
η_{turbin}	*Turbine efficiency*	*0.85%*
P_8	*Inlet pressure to turbine NO. 2*	2300 kPa
P_{10}	*Inlet pressure to pump NO. 2*	1300 kPa
η_{pump}	*Pump efficiency*	*0.8%*

4.1.1. Electrolyzer PEM

In the proposed system, an Electrochemical Proton Exchange Membrane (EPEM) has been utilized for the production of hydrogen. Hydrogen, in its diatomic form (H2), is not readily available in nature and must be produced using specific equipment [32]. Electrolyzers are one of the devices commonly used for hydrogen production, offering distinct advantages such as rapid production and high efficiency [33,34]. The electricity needed to power the electrolyzer in the geothermal system of this research is sourced from the organic Rankine cycle. This integration allows the system to efficiently produce hydrogen using renewable energy sources. For a more detailed understanding of the relationships and the functioning of the electrolyzer, you can refer to relevant previous references [33–35].

4.1.2. System balance

To balance the energy and cost aspects of the system under investigation in this research, the relationships and equations provided in Table 3 are applied. These relationships likely help in optimizing the system's performance and making it more cost-effective.

In addition to the previously mentioned strategies, the system enhances its net power output during periods of peak energy demand by utilizing electricity generated from a fuel cell. This additional source of electricity generated by the fuel cell further contributes to meeting high-demand energy requirements efficiently.

$$\dot{W}_{net-Pick} = \dot{W}_{ORC} + \dot{W}_{FC} \tag{1}$$

4.1.3. Efficiency

Exergy efficiency is calculated according to equation (2):

$$\eta_{ex} = \frac{(\dot{W}_{net} + \dot{W}_{FC} + Q_{cooling})}{\dot{E}x_1 + (\dot{n}_{H2} \times hhv_{H2})} \times 100 \tag{2}$$

Table 3
Relationships related to energy balance and system exergy.

System components	Energy balance	Exergy balance
ORC Turbine NO. 1	$\dot{W}_{tur1} = (\dot{m}_4 \times ((h_4 - h_5)$	$\dot{E}x_{tur1} = \dot{E}x_4 - \dot{E}x_5 - \dot{W}_{tur1}$
Evaporator	$Q_{eva} = \dot{m}_1 \times (h_1 - h_2)$	$\dot{E}x_{eva} = \dot{E}x_1 + \dot{E}x_7 - \dot{E}x_2 - \dot{E}x_4$
ORC pump NO. 1	$\dot{W}_{pump1} = \dot{m}_6 \times (h_7 - h_6)$	$\dot{E}x_{pump1} = \dot{E}x_6 + \dot{W}_{pump1} - \dot{E}x_7$
Heat exchanger	$Q_{HEX} = \dot{m}_5 \times (h_5 - h_6)$	$\dot{E}x_{HEX} = \dot{E}x_5 + \dot{E}x_{11} - \dot{E}x_8 - \dot{E}x_6$
ORC pump NO. 2	$\dot{W}_{pump2} = \dot{m}_{10} \times (h_{11} - h_{10})$	$\dot{E}x_{pump2} = \dot{E}x_{10} + \dot{W}_{pump2} - \dot{E}x_{11}$
ORC Turbine NO. 2	$\dot{W}_{tur2} = (\dot{m}_8 \times ((h_8 - h_9)$	$\dot{E}x_{tur2} = \dot{E}x_8 - \dot{E}x_9 - \dot{W}_{tur2}$
Condenser	$Q_{cond} = \dot{m}_9 \times (h_9 - h_{10})$	$\dot{E}x_{cond} = \dot{E}x_9 + \dot{E}x_{12} - \dot{E}x_{10} - \dot{E}x_{13}$
Organic Rankine Cycle	$\dot{W}_{ORC1} = \dot{W}_{\dot{W}_{tur1}} - \dot{W}_{pump1}$	$\dot{E}x_{ORC1} = \dot{E}x_{tur1} + \dot{E}x_{pump1} + \dot{E}x_{eva} - \dot{E}x_{HEX}$
	$\dot{W}_{ORC2} = \dot{W}_{\dot{W}_{tur2}} - \dot{W}_{pump2}$	$\dot{E}x_{ORC2} = \dot{E}x_{cond} + \dot{E}x_{pump2} + \dot{E}x_{tur2} + \dot{E}x_{HEX}$
Total system	$\dot{W}_{net} = \dot{W}_{ORC1} + \dot{W}_{ORC2}$	$\dot{E}x_{net} = \dot{E}x_{ORC1} + \dot{E}x_{ORC2}$

4.2. System economic analysis

The relations related to the calculation of system equipment cost are introduced in Table 4 [36].

4.3. Topsis method

The TOPSIS method is a decision-making approach used to evaluate and select the best alternatives based on predefined criteria. It involves comparing each alternative to both an ideal solution and a negative ideal solution within the target space, as illustrated in the figure. To apply the TOPSIS method effectively, the steps outlined in Fig. 3 must be followed [37,38].

4.4. Response surface optimization (RSM) method

The Level method is a statistical technique used for constructing experimental models. It is employed to optimize a response variable that is affected by various design parameters. This method involves conducting a series of tests, during which changes are made to the input variables in each test to determine how these changes impact the response variable. Experimental design aims to calculate the optimal values for decision variables and objective functions. Fig. 4 provides an overview of the solution flowchart for the Response Surface Method (RSM) [39,40].

Table 4
Cost rate equation of system components.

Components	Relation
Organic Rankine Cycle Turbine NO. 1	$Z_{tur1} = (4750 \times (\dot{W}_{tur1}{}^{0.7}) + 60 \times (\dot{W}_{tur1}{}^{0.95})) \times \dot{Z}$
ORC Turbine NO. 2	$Z_{tur2} = (4750 \times (\dot{W}_{tur2}{}^{0.7}) + 60 \times (\dot{W}_{tur2}{}^{0.95})) \times \dot{Z}$
PEMFC	$Z_{PEMFC} = 1000 \times \dot{W}_{FC}$
EPEM	$Z_{PEME} = 1000 \times \dot{W}_{PEME}$
Evaporator	$Z_{eva} = 276 \times (A_{eva}{}^{0.88}) \times \dot{Z}$
Heat exchanger	$Z_{HEX} = 12000 \times \left(\frac{A_{HEX}}{100}\right)^{0.6} \times \dot{Z}$
Condenser	$Z_{Cond} = 1773 \times \dot{m}_9 \times \dot{Z}$
ORC pump NO. 1	$Z_{Pump1} = 3500 \times (\dot{W}_{Pump1}{}^{0.41}) \times \dot{Z}$
ORC pump NO. 2	$Z_{Pump2} = 3500 \times (\dot{W}_{Pump2}{}^{0.41}) \times \dot{Z}$

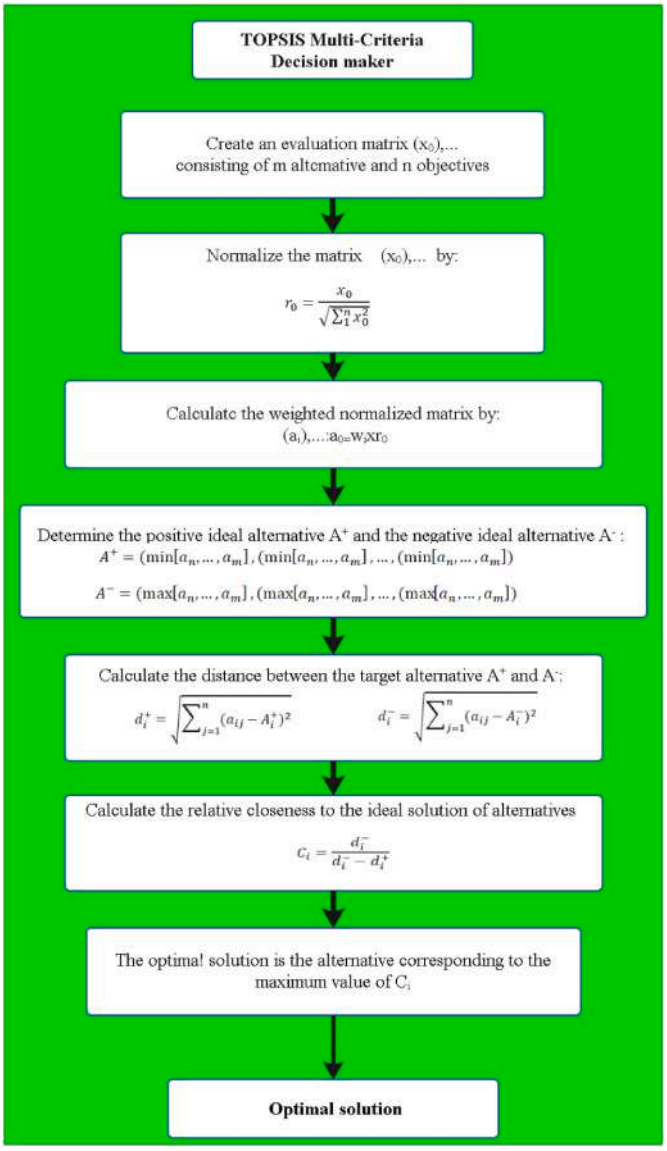

Fig. 3. Flowchart of TOPSIS method.

5. Results

5.1. Electrolyzer PEM validation

To ensure the reliability of the simulation results and validate the work conducted, a validation analysis was carried out prior to the system analysis. Since the introduced geothermal system is novel, the validation of the EPEM subsystem was evaluated using the research findings of Ioroi et al. [41]. Fig. 5 illustrates the comparison of simulation results with the referenced research. These results demonstrate that this research has strong validity, indicating that the simulation process is reliable, and the outcomes are accurate and trustworthy.

5.2. Analysis of organic fluids

This research involved the investigation of various scenarios aimed at identifying the optimal choice of organic fluids for the two Rankine cycles. These scenarios were evaluated using Sankey analysis to determine the most suitable scenario that maximized system performance. Fig. 6 presents the Grossman diagram created through Sankey analysis for the six predefined scenarios. The details of these scenarios can be found in Table 5.

The results of the exergy destruction rate analysis for the components of the system revealed that the ORC 1 has the highest exergy destruction rate, with the evaporator and the turbine of the ORC 1 being the specific components contributing most to this exergy destruction. Following this, the ORC 2, EPEM, and chiller unit exhibited relatively high exergy destruction, while the FC unit had the lowest exergy destruction rate.

It's worth noting that pumps 1 and 2 consistently displayed the lowest exergy destruction in all analyses. In the scenarios, geothermal energy enters the system with an exergy rate of 2795.6–3320.4 kWh. This geothermal energy is utilized by the evaporator to power the ORC 1 and the absorption chiller. Subsequently, a heat exchanger supplies the energy needed by organic Rankine cycle No. 2 for electricity generation.

The analysis also demonstrated that in all scenarios, the production power falls within the range of 1082–1258 kWh, while the exergy destruction rate of the system ranges from 1568.5 to 1901.9 kWh.

The role of new and renewable energies in electrical power generation has gained increasing importance. In addition to geothermal energy, fuel cell technology has become a significant contributor. The production power calculated in this section represents the sum of the production power from the ORC turbines and the fuel cell unit, specifically during periods of peak consumption.

The variations in the six examined scenarios pertain to the choice of organic fluids used in the two organic Rankine cycles and their impact on the production power and the exergy destruction of the system. As depicted in Fig. 7, the scenario with the highest production power is Scenario 2, while Scenario 1 yields the lowest production power. A comparison of these two scenarios illustrates that a significant effect on the system's production power can be achieved by altering the organic fluid of ORC No. 1. In this instance, the organic fluid used in cycle No. 2 is R115 refrigerant in both scenarios, indicating that the change in power production rate solely resulted from changing the organic fluid in cycle No. 1.

The results presented in Fig. 8 indicate that the scenario with the highest exergy destruction is Scenario 5, while Scenario 1 exhibits the lowest exergy destruction. Interestingly, Scenario 1, which has the lowest production and performance power, also displays the lowest exergy destruction rate. This suggests that, while Scenario 1 is not the most productive, it operates with a higher degree of thermodynamic efficiency, resulting in lower exergy destruction.

Sankey analysis further highlights that the primary contributors to exergy destruction within the system are ORC 1 and ORC 2 units. Selecting the right organic fluid for these cycles can significantly reduce the exergy destruction rate and, consequently, enhance the system's production power.

Based on the analysis and the use of the TOPSIS method to evaluate various scenarios, Scenario No. 3 was identified as the most favorable option for the system. This scenario demonstrates a good balance between production power and exergy destruction rate, making it a suitable choice. Table 6 provides the details of the best scenario.

After conducting Sankey analysis, which is a valuable tool for determining the best scenarios in studies, and applying the TOPSIS method, Scenario 3 was identified as the most optimal scenario. This scenario exhibits the highest production power and the lowest exergy destruction rate, making it the preferred choice for further analysis.

Fig. 9 provides insight into the production power and power consumption of the system's components for the best scenario. The results indicate that ORC turbine No. 1 generates the highest production power within the geothermal system, followed by ORC turbine No. 2. In contrast, the fuel cell unit, which has been integrated into the geothermal system for peak consumption periods, exhibits the lowest production power. It's worth noting that this unit is powered by hydrogen produced within the system. Additionally, the power consumption of pump No. 1, pump No. 2, and the EPEM unit is covered by the productive power generated by the geothermal system. This research underscores the efficiency of Rankine cycles, as demonstrated by the low

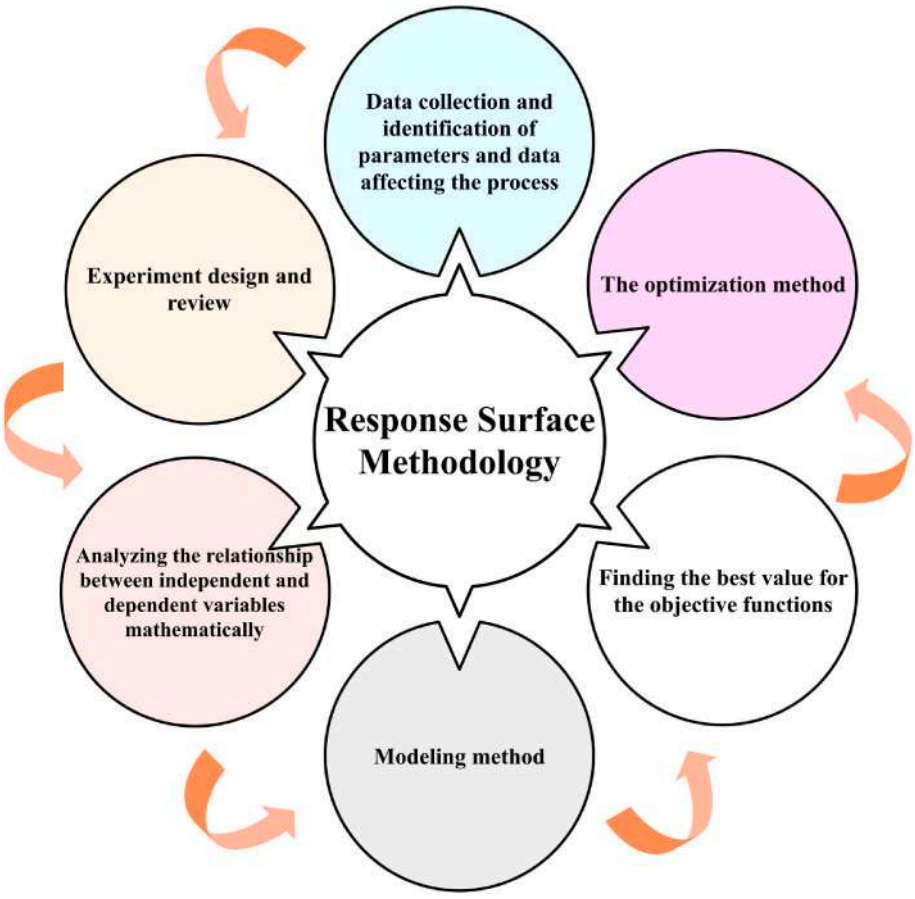

Fig. 4. RSM method flowchart.

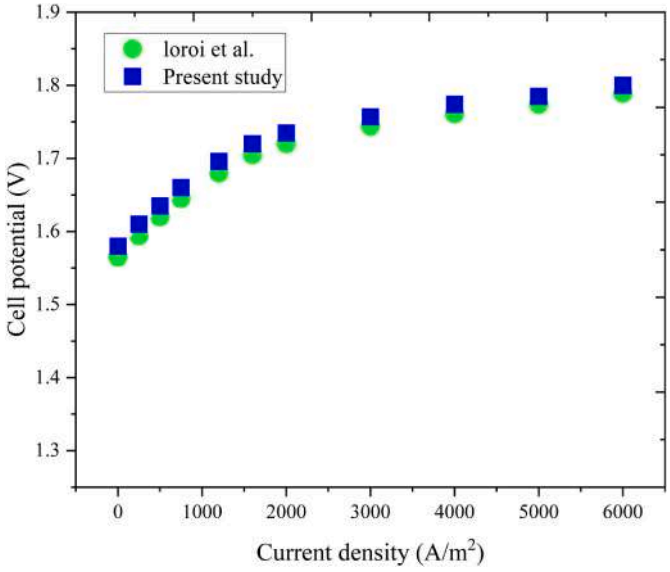

Fig. 5. Validation.

power consumption of the pumps.

In Fig. 10, the exergy degradation of the various components within the system is analyzed for the best scenario. The results reveal that the highest exergy degradation occurs in the solar unit and the parabolic collector. Following closely is the Rankin cycle unit No. 1, which includes four components: the evaporator, turbine, pump, and heat exchanger. Conversely, the fuel cell unit exhibits the lowest exergy degradation within the system. This information provides insights into areas where improvements or optimization efforts could be directed to further enhance system efficiency.

5.3. Optimization

In the optimization of this research, the RSM is employed to determine the most optimal values for the objective functions. The optimization process involves seven influential design parameters as optimization variables. Three objective functions, namely exergy efficiency, hydrogen production, and system cost rate, were chosen to enhance the system's performance. The goal is to increase efficiency and hydrogen production while reducing the system cost rate. Table 7 provides an overview of the seven decision variables selected as design parameters that impact the system's performance, along with their respective ranges.

The Design of Experiments method involves conducting tests with deliberate variations in the input variables to observe their impact on the response variables and determine the reasons for these changes. In the DOE process, several initial variables (optimization variables) are tested to assess their effect on the response variable (objective functions) within specified upper and lower bounds. These bounds are defined based on reference articles, system performance conditions, and equipment standards.

In Appendix 1, the optimal points for the objective functions are presented, along with the values of the optimization variables. These values were determined using the Design Expert software, and the best optimal points were selected to enhance the technical and economic performance of the system. Each of these points has a desirability value, with the desirability value of point 1 being 0.646%, which is higher than the other points. The closer the desirability value is to 1, the more

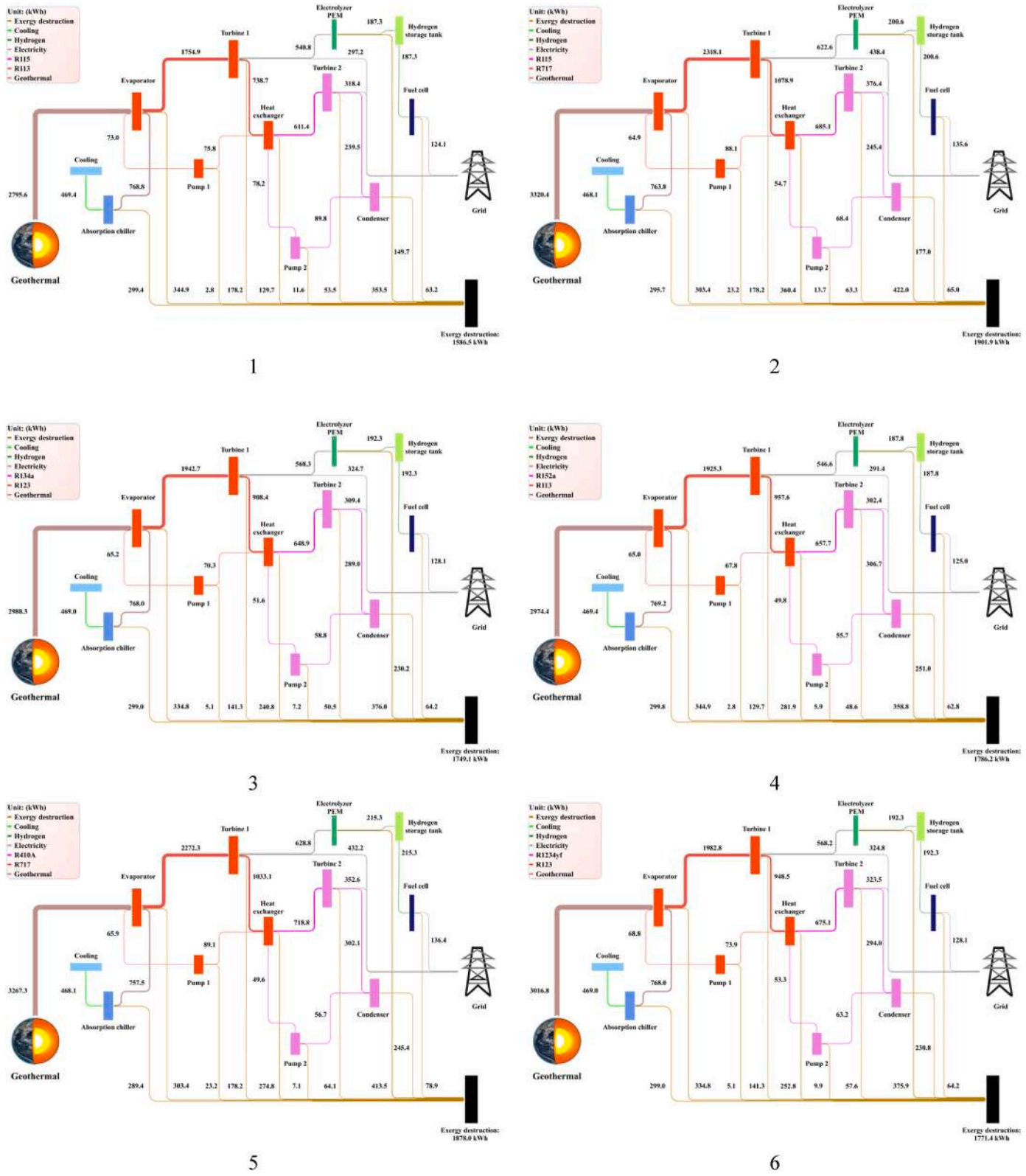

Fig. 6. Grossman system diagram for organic fluids.

acceptable the result.

In this research, 7 decision variables and 3 objective functions were chosen, and optimizing these parameters can contribute to improving the technical efficiency and reducing the economic costs of the system.

In optimization using the RSM, 100 optimal points were calculated. Among these points, the first solution is considered the best and most optimal. The optimal results for the 88 legs in the modeling process using the response level method for decision variables and objective functions are detailed in Table 8.

The effect of changes in design parameters on efficiency is shown in Fig. 11. The exergy efficiency of the system in optimization ranges from 50% to 90%. All variables work together to reach an exergy efficiency of

Table 5
Scenarios examined.

Scenarios	Organic fluid cycle N0. 1	Organic fluid cycle NO. 2
1	*R113*	*R115*
2	*R717*	*R115*
3	*R123*	*R134a*
4	*R113*	*R152a*
5	*R717*	*R410A*
6	*R123*	*R1234yf*

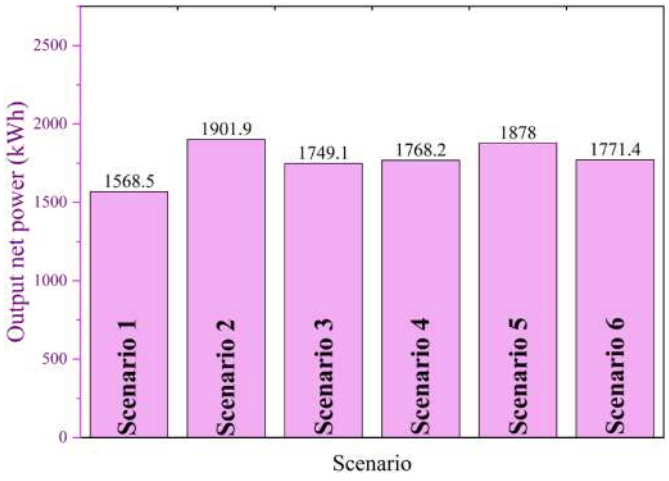

Fig. 7. Production power under the six scenarios.

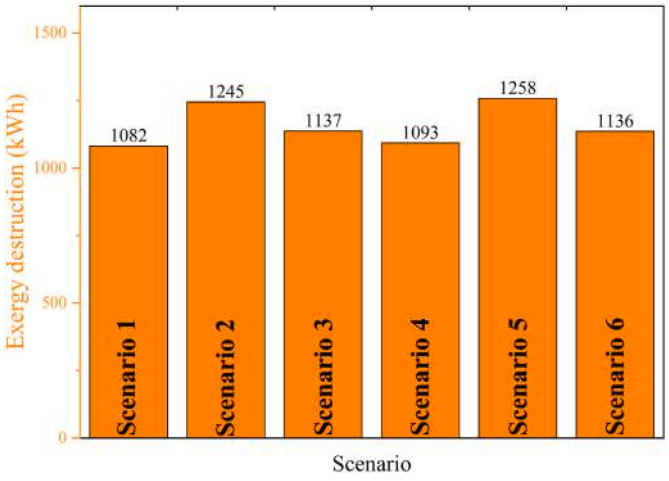

Fig. 8. Analysis of the exergy destruction of scenarios.

Table 6
Selection of the best scenario.

Scenario	Organic fluid cycle NO. 1	Organic fluid cycle NO. 2	Peak Power (kWh)	Total exergy destruction (kWh)
Scenario 3	*R123*	*R134a*	*1137*	*1749.1*

81.816%, which is considered the optimal value. The results reveal that the temperature in the evaporator, $turbine_{efficiency}$, to pump $1_{inlet\ temperature}$, and $Geothermal_{mass\ flow\ rate}$ are among the most influential design parameters. Increasing these parameters has a significant impact on enhancing the exergy efficiency of the entire system.

It's important to note that the evaporator and turbine are the key components of the system. The evaporator provides the thermal energy needed by the ORC to generate electricity, and the turbine produces power. Therefore, changes in input parameters for the evaporator and turbine, as the two main components of the system, have a substantial effect on improving overall system efficiency. The results presented in the optimal state highlight the simultaneous impact of two design parameters on the exergy efficiency objective function.

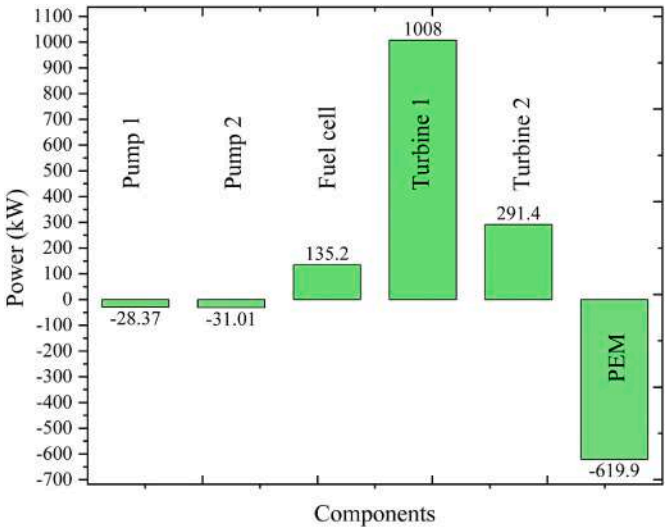

Fig. 9. Power generation and consumption rates under the optimal scenario.

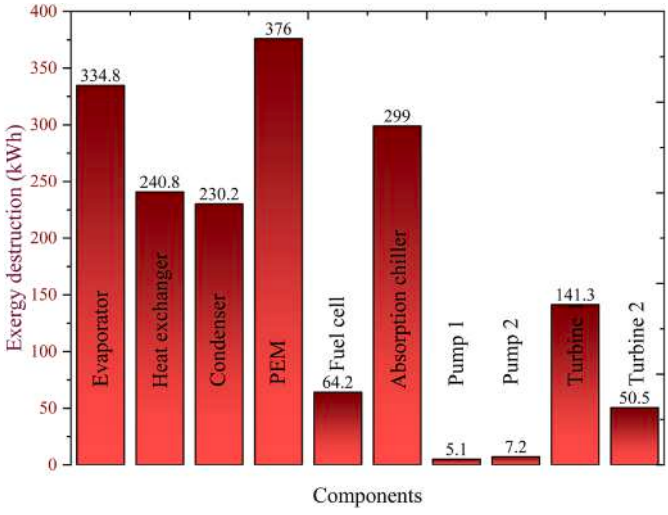

Fig. 10. Exergy destruction rates under the optimal scenario.

Table 7
Optimization variables and range.

Factor	Decision variables	lower bound	Upper bound
a	*Pump efficiency (%)*	*0.7*	*0.95*
b	*Turbine efficiency (%)*	*0.7*	*0.95*
c	*Pinch point evaporator (^{0}C)*	*3*	*10*
d	*Mass flow rate geothermal (kg/s)*	*5*	*25*
e	*T1 (^{0}C)*	*170*	*220*
f	*T4 (^{0}C)*	*100*	*140*
g	*T6 (^{0}C)*	*30*	*50*

The effect of changes in design parameters on cost rate is shown in Fig. 12. The optimization of the system cost rate is crucial in designing and implementing a system, ensuring not only its functionality but also its affordability. By optimizing this objective function, it becomes possible to design a system that operates at an acceptable cost.

The results indicate that in multi-objective optimization, the range of

Table 8
Optimum value.

Number	Pump efficiency (%)	Turbine efficiency (%)	Pinch point evaporator (^{0}C)	Mass flow rate geothermal (kg/s)	T1 (^{0}C)	T4 (^{0}C)	T6 (^{0}C)	Exergy efficiency (%)	Cost rate ($/h)	Hydrogen (kg/h)	Desirability (%)
1	*0.884*	*0.902*	*4.54*	*8.852*	*210.253*	*132.245*	*33.852*	*81.816*	*15.967*	*25.119*	*0.646*

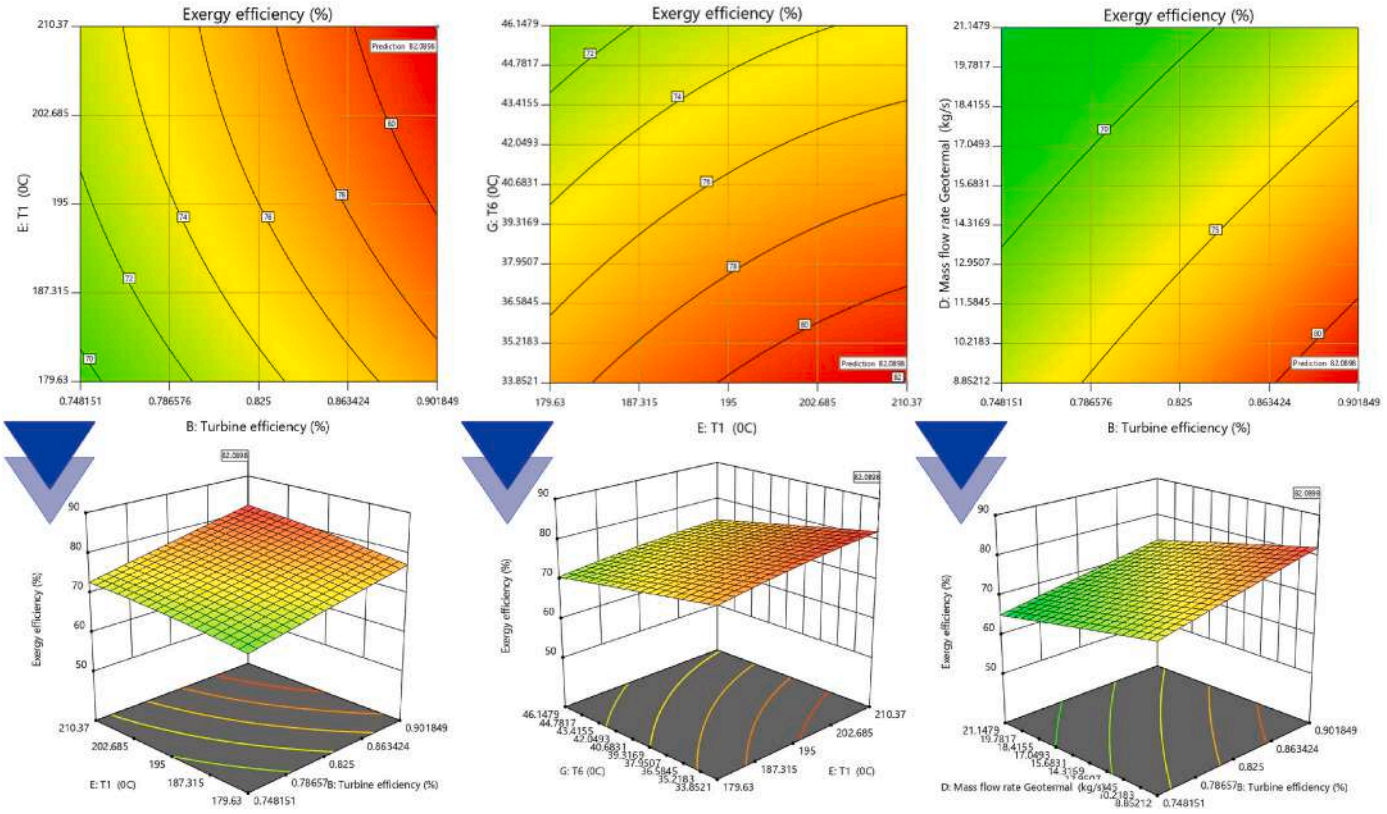

Fig. 11. Exergy efficiency versus optimization variables.

the system cost rate is between 5 and 30 $/h. All variables are striving to achieve a system cost rate of 15.967 $/h, which is considered the optimal value. In other words, optimizing this objective function can significantly reduce the system's cost to an acceptable level, roughly halving the cost rate.

The findings in Fig. 12 reveal that four parameters—turbine$_{\text{efficiency}}$, evaporator$_{\text{pinch point}}$, evaporator$_{\text{inlet temperature}}$, and Geothermal$_{\text{mass flow rate}}$—are among the most influential design variables. These parameters have a substantial impact on increasing or decreasing the cost rate objective function. The optimization process using the RSM method demonstrates how much the acceptable value of these parameters can be improved.

He effect of changes in design parameters on hydrogen production is shown in Fig. 13. The hydrogen production plays a critical role in ensuring an adequate supply of clean fuel. The range of the hydrogen production is between 0 kg/h and 50 kg/h. All variables are striving to achieve a hydrogen production of 25.119 kg/h, which is considered the optimal value. In other words, by optimizing, it's possible to significantly enhance the acceptable rate of hydrogen produced by the system as a clean fuel. The findings presented in Fig. 13 illustrate that four parameters—turbine$_{\text{efficiency}}$, evaporator$_{\text{pinch point}}$, evaporator$_{\text{inlet temperature}}$, and Geothermal$_{\text{mass flow rate}}$—are among the most influential decision variables when it comes to increasing the hydrogen production.

5.4. Forecasting optimized objective functions

The performance and behavior of the three objective functions were analyzed individually using a genetic regression algorithm.

A regression equation for the objective function of exergy efficiency rate and geothermal system cost rate was derived to calculate the cost behavior in subsequent system calculations.

The performance and behavior of the three objective functions were analyzed individually using a genetic regression algorithm. A regression equation for the objective function of exergy efficiency rate, hydrogen production and geothermal system cost rate was derived to calculate the cost behavior in subsequent system calculations. For simplification, the design parameters were represented by English letters, as detailed in Table 9.

The analysis of the obtained regression relationships is used for estimating or predicting the relationships between variables. It helps in calculating the relationship between the design parameters and the objective functions, which, in turn, assists in determining the solution process for the objective functions when the values of the design parameters are altered. In essence, regression analysis is employed to comprehend the relationship between design parameters and target functions.

The regression relationship of system exergy efficiency is obtained according to equation (3), and the coefficients of exergy efficiency

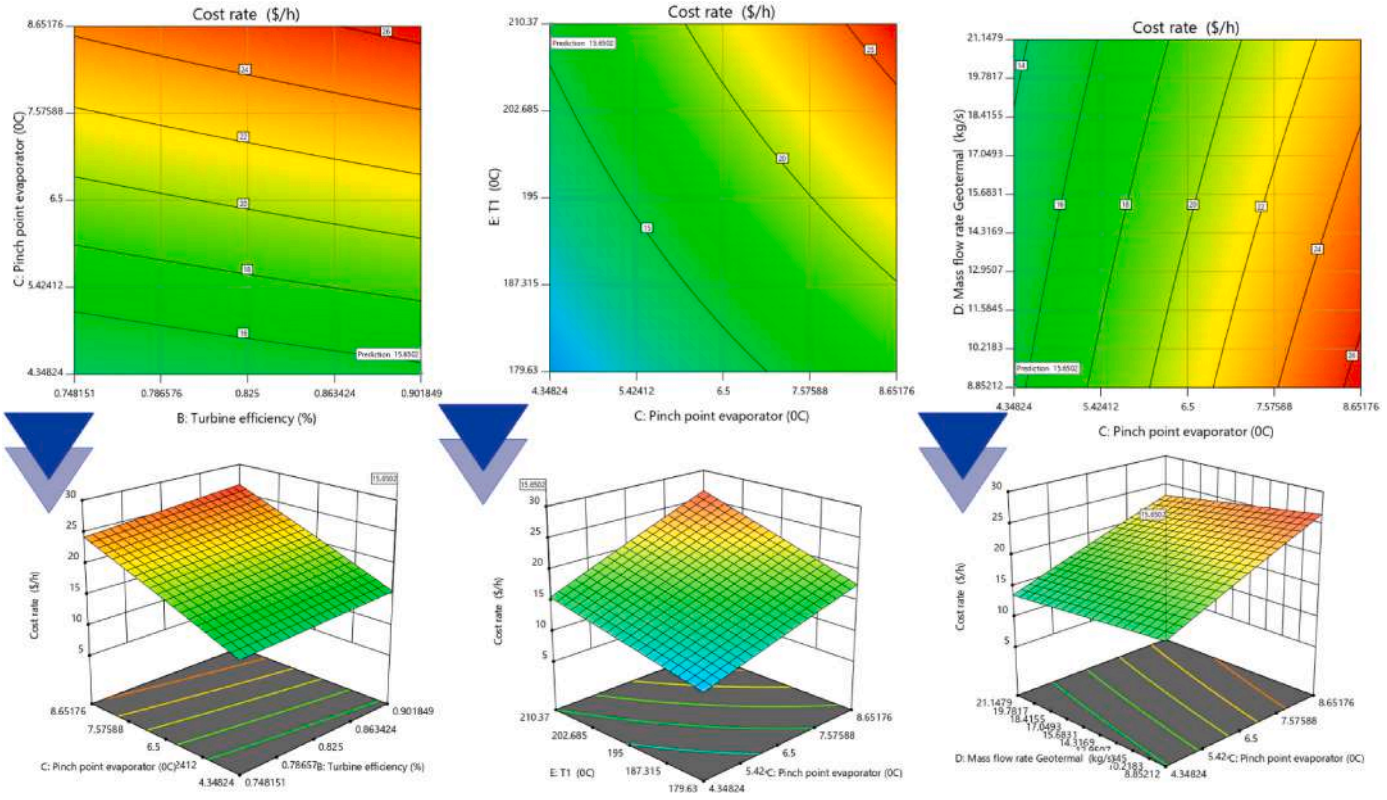

Fig. 12. Cost rate versus optimization variables.

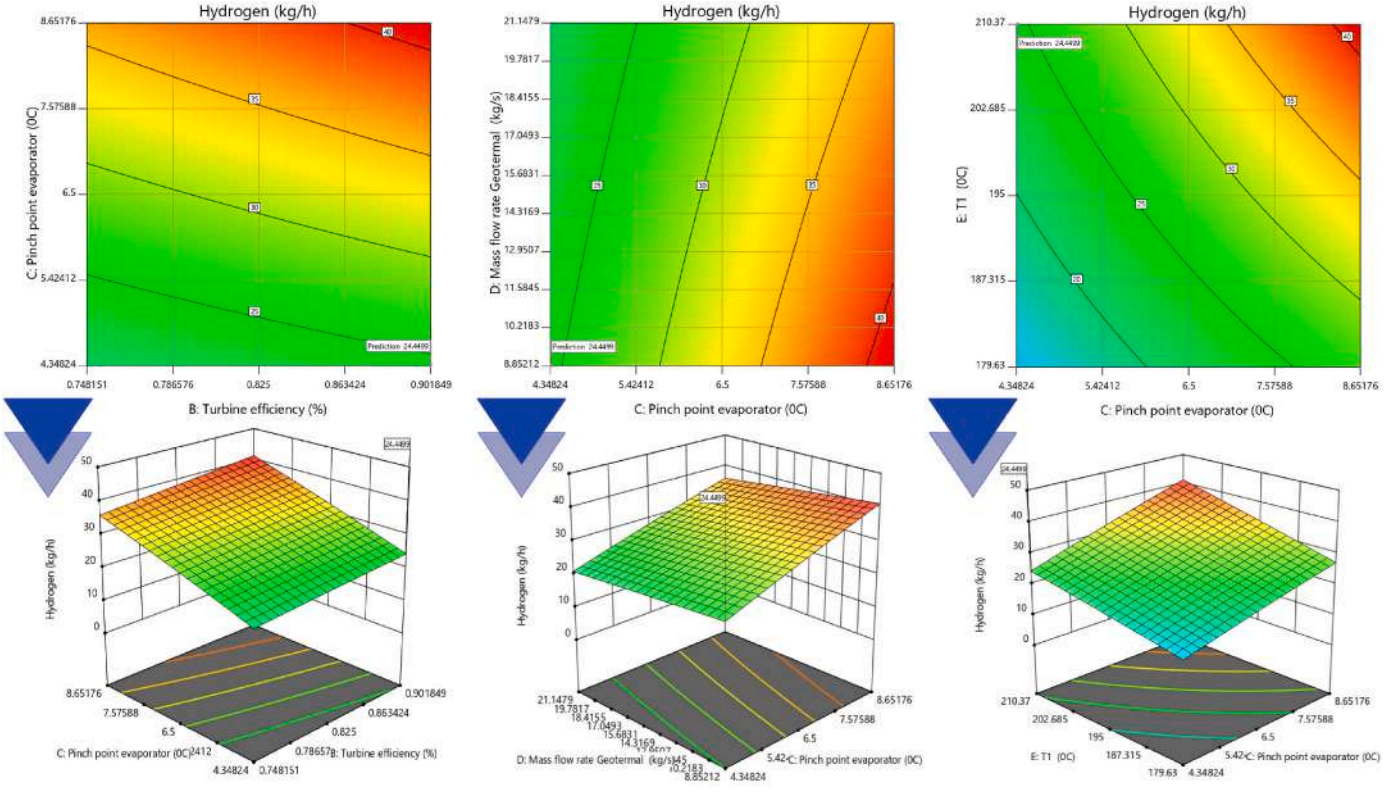

Fig. 13. Hydrogen rate production versus optimization variables.

Table 9
Simplification of regression relations.

Decision variables	Symbol
Pump efficiency (%)	*W1*
Turbine efficiency (%)	*W2*
Pinch point evaporator (^0C)	*W3*
Mass flow rate geothermal (kg/s)	*W4*
T1 (^0C)	*W5*
T4 (^0C)	*W6*
T6 (^0C)	*W7*

Table 10
Exergy efficiency.

Coefficient	Valve	Coefficient	Valve
a_1	*14.53*	a_{12}	*1.93*
a_2	*6.77*	a_{13}	*15.55*
a_3	*0.66*	a_{14}	*1.11*
a_4	*0.37*	a_{15}	*10.15*
a_5	*0.48*	a_{16}	*1.99*
a_6	*0.21*	a_{17}	*17.50*
a_7	*4.72*	a_{18}	*5.03*
a_8	*1.73*	a_{19}	*1.60*
a_9	*2.12*	a_{20}	*0.42*
a_{10}	*6.07*	a_{21}	*102.01*
a_{11}	*12.21*		

equation are introduced in Table 10.

Table 11
Cost rate.

Coefficient	Valve	Coefficient	Valve
b_1	*0.76*	b_{12}	*0.12*
b_2	*0.14*	b_{13}	*2.07*
b_3	*0.72*	b_{14}	*1.40*
b_4	*1.02*	b_{15}	*15.64*
b_5	*0.08*	b_{16}	*0.76*
b_6	*2.03*	b_{17}	*13.84*
b_7	*14.93*	b_{18}	*0.32*
b_8	*19.31*	b_{19}	*19.38*
b_9	*0.63*	b_{20}	*0.92*
b_{10}	*15.57*	b_{21}	*0.0004*
b_{11}	*0.37*	b_{22}	*4.69*

Table 12
Production rate of hydrogen.

Coefficient	Valve	Coefficient	Valve
c_1	*2.52*	c_{13}	*12.96*
c2	*0.54*	c_{14}	*0.99*
c_3	*1.71*	c_{15}	*2.21*
c_4	*2.30*	c_{16}	*1.04*
c_5	*16.96*	c_{17}	*1.87*
c_6	*1.25*	c_{18}	*12.13*
c_7	*14.79*	c_{19}	*1.45*
c_8	*0.59*	c_{20}	*14.25*
c_9	*4.54*	c_{21}	*2.84*
c_{10}	*19.57*	c_{22}	*1.34*
c_{11}	*17.49*	c_{23}	*24090.64*
c_{12}	*0.85*	c_{24}	*52.52*

$$\textit{Exergy efficiency} = (((((a1/(a2)\times((a3\times W7/(a4\times W2)-a5\times W2*a6\times W3)+(-a7/(-a8)-a4\times W1*a9\times W1))+(a1/(-a8)\times a9\times W7\times a10+(-a7/(-a8)-(a11-a5)))\times a4\times W2\times a9\times *W2/((a12\times W4-a13))/((a14\times W6/(a15)+(a16\times W7-a13)))))/((-a17))-a18)+a3\times W7/(a4\times W1))+(a12\times W4-a13))/(a19\times W2)\times(-a20)+a21) \quad (3)$$

The system cost rate regression relationship is obtained according to equation (4), the coefficients of cost rate equation are introduced in Table 11.

$$\textit{Cost rate}=(((((b1\times W5-(-b2-b3\times W7))-(b4\times W4+b5\times W2))+(((b1\times W5-(b4\times W4+b5\times W1))-EXP(b6))-(((-b2-b3\times W7)-b7)+(b5\times W1-b8)))/((((b9\times W7-b10)-((b11\times W3+b12\times W2)+b12\times W1)\times b13\times W6/((b14\times W3+b15)))-(b11\times W3+b12\times W2)*(b11\times W3-b12\times W1)))))\times((EXP(b6)-(b11\times W3+b12\times W2)\times(b16\times W5-(b17+b18\times W6)))-(((b19\times W2+b19\times b20\times W1)+(b17+b18\times W6))+((b17+b18\times W6)+b18\times W6))/((b4\times W4+b5\times W2)))-b1\times W5)\times(-b21)+b22) \quad (4)$$

The regression relationship of hydrogen production of the system is obtained according to equation (5), the coefficients of this equation are presented in Table 12.

$$\textit{Hydrogen}=(c1/(((c2\times W4*(c3\times W4-c4\times W7/(-c5)/((-c6\times W3-c7)))-(((c8\times W6/(-c9)-c10)-c11)-(c12\times W7-(((((-c13-c14\times W5)-EXP(c15\times W3))+(c16\times W1-c17*W3)/((-c7+c18)))+c19*W6)-((-c7-c14*W5)+(-c20-c7))*((-c20-c7)-c21*W7*c2)/(c8*W4*EXP(c9)))))*(EXP(c15*W3)+c22*W4)))*c23+c24) \quad (5)$$

The results of predicting the behavior of the investigated objectives for two modes of testing and training in the optimal state of the system are calculated in Fig. 14. In this analysis, eighty percent of the data was allocated for training, while twenty percent was used for testing to ensure the correct solution to the problem. The goal is to achieve the best and most optimal value, which is represented by the objective function line.

The relationship between the actual value and the estimated value of the objective functions is calculated in Fig. 15. This graph contains

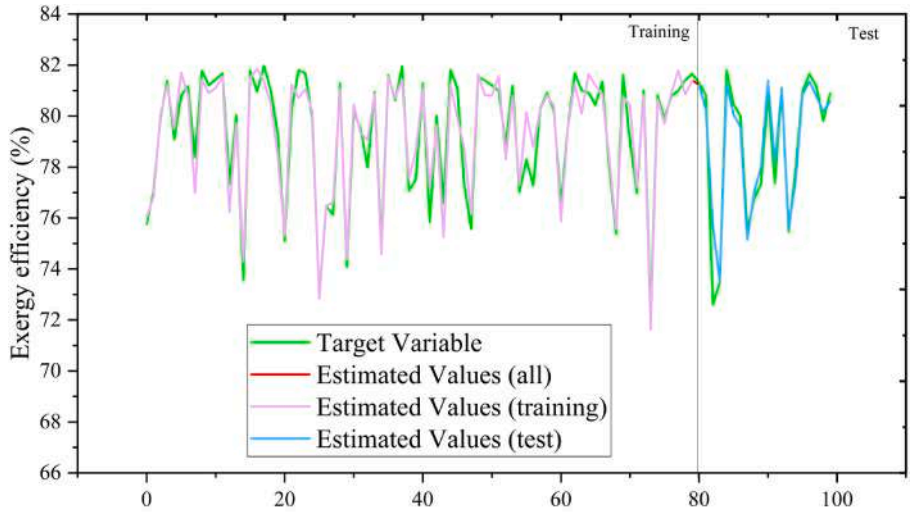

a. Exergy efficiency

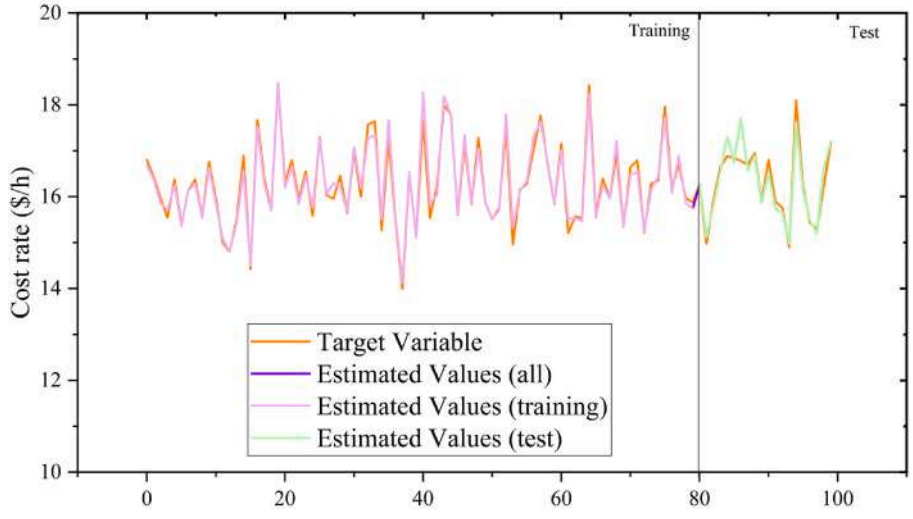

b. Cost rate

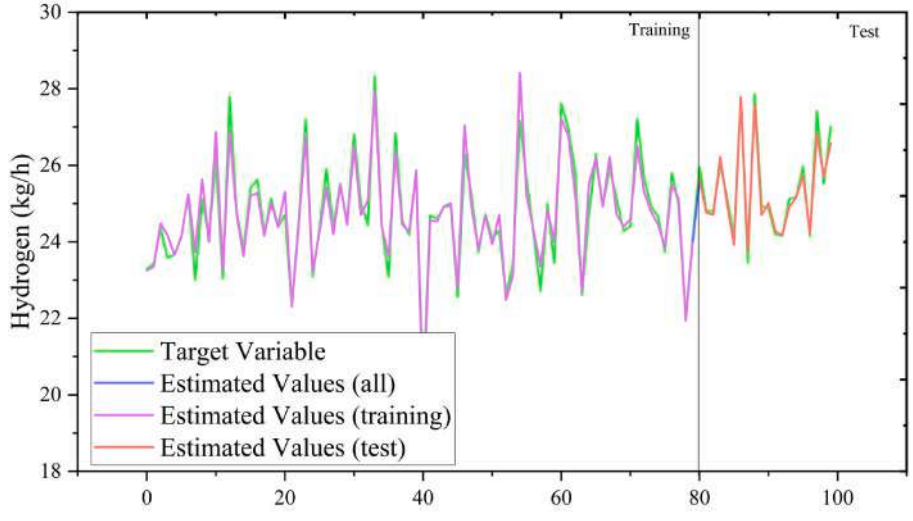

C: Hydrogen

Fig. 14. Predicting the behavior of functions.

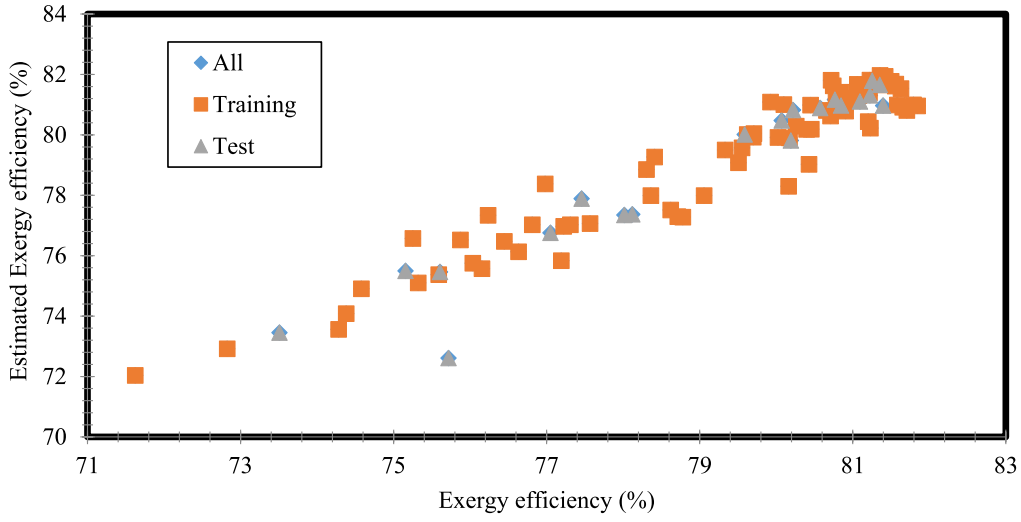

a. Exergy efficiency

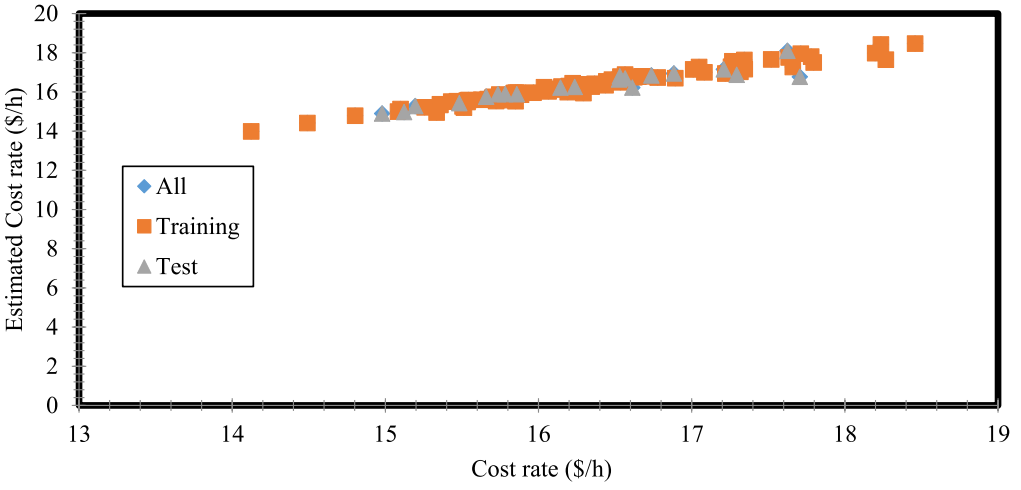

b. Cost rate

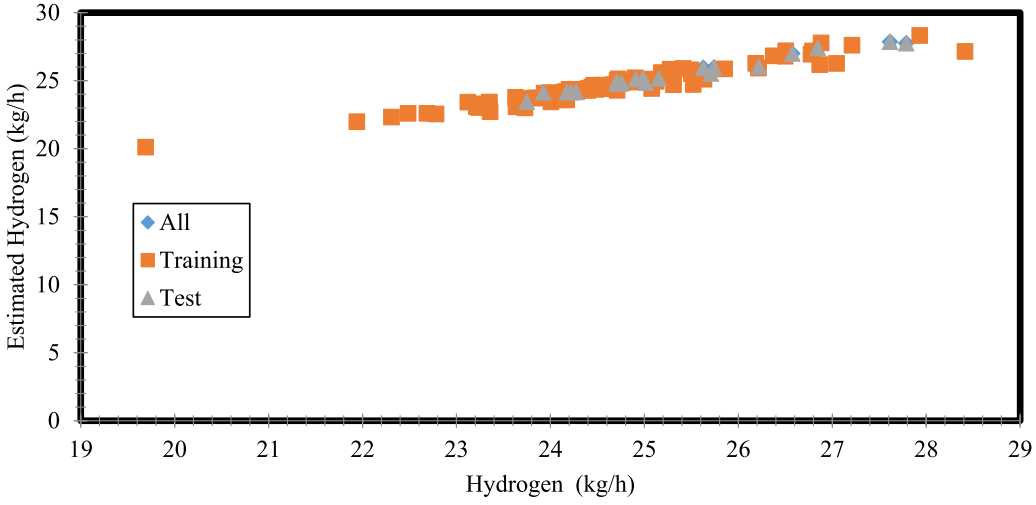

C: Hydrogen

Fig. 15. Estimating the change trend of objective functions.

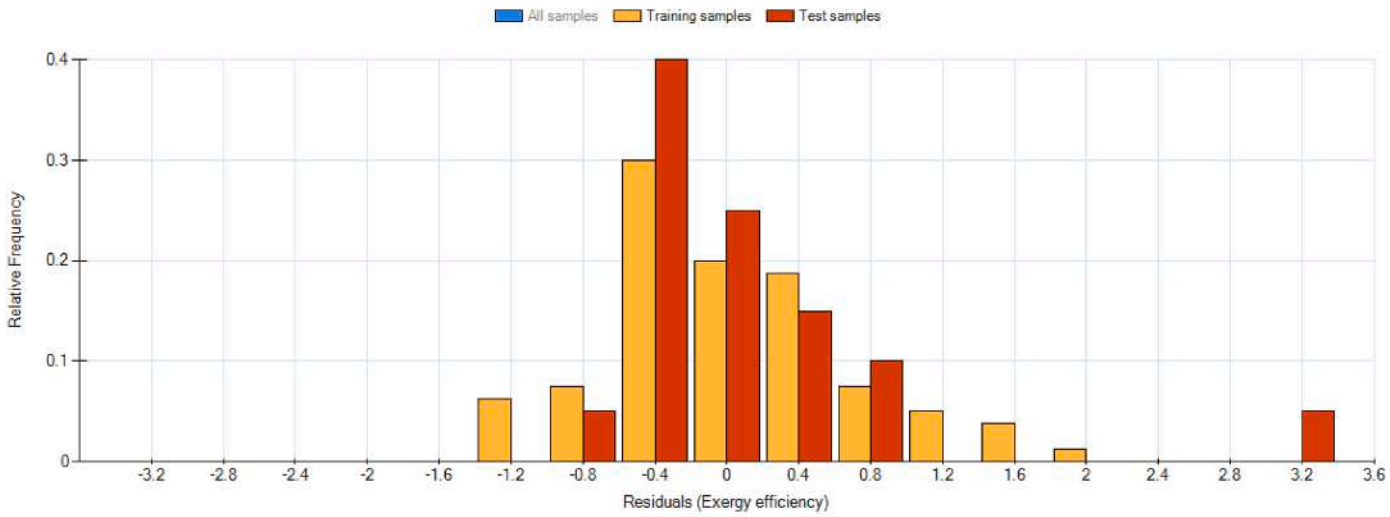

a. Exergy efficiency

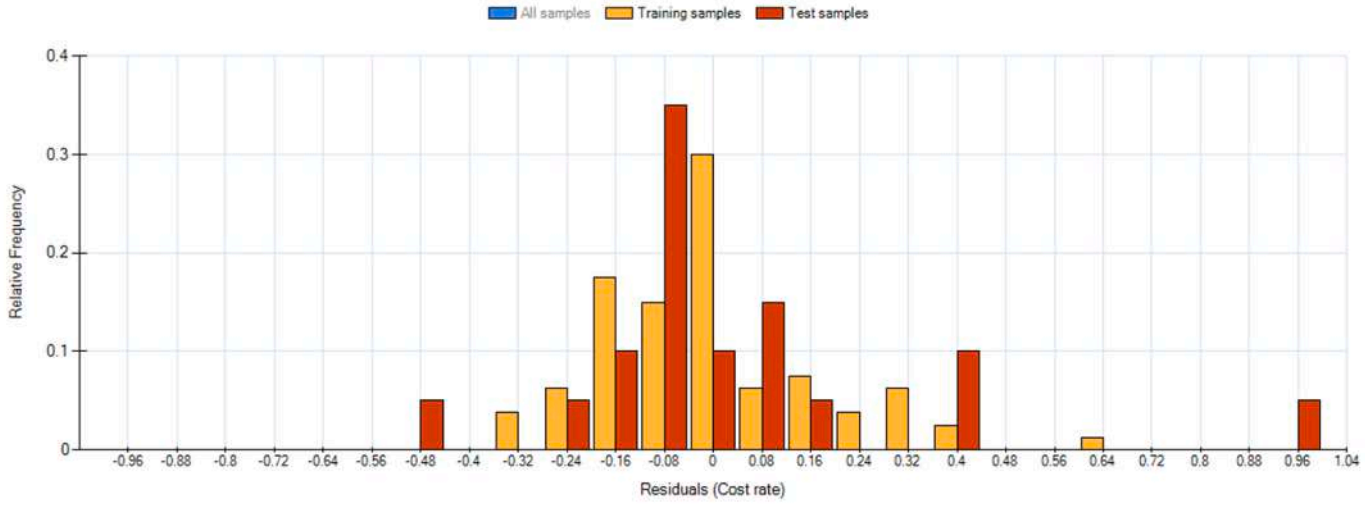

b. Cost rate

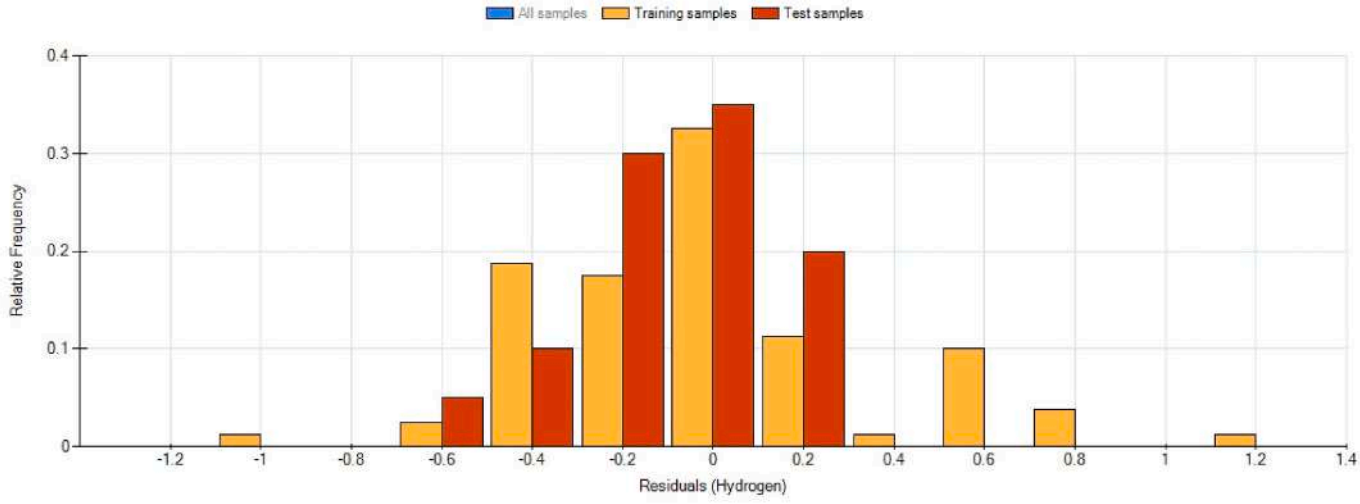

C: Hydrogen

Fig. 16. Histogram diagram.

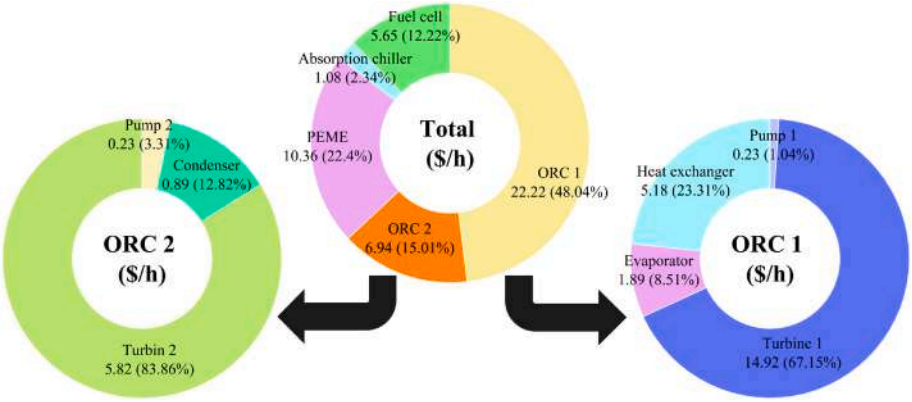

Fig. 17. Cost rate of units and various components of the system.

various data points for the objective function throughout the solution process. The closer the actual and estimated objective function values are, the better the model performance. When the actual and estimated values overlap, it shows the best result for the two objective functions.

Fig. 16 presents histograms of the three objective functions for both the training and testing processes. The horizontal axis represents the values of the objective functions, while the vertical axis shows the percentage frequency. A histogram is essentially a column chart that provides insight into the distribution of quantitative variables. Each column's height corresponds to the frequency or percentage frequency of values falling into specific categories. By using histograms and superimposing a normal distribution curve, you can gain a better understanding of the distribution pattern of the variable in question.

5.5. Economic analysis

The cost calculation of study system components and units is done in Fig. 17. The study system units are categorized into five distinct sections, which include the EPEM unit, FC unit, and ORC 1 and 2, as well as the chiller. The cost rate of the entire system has been calculated at 46.25 $/h. Notably, the ORC 1 unit carries the highest system cost rate, totaling 22.22 $/h. It is followed by the EPEM unit with a cost rate of 10.36 $/h, and the ORC 2 unit with a cost rate of 6.94 $/h. In terms of individual components, the cost rate analysis reveals that the turbine1, turbine2, HEX, evaporator, and condenser components bear the highest cost rates. In contrast, the pump components exhibit the lowest cost rates among all system elements (see Fig. 17).

6. Case study

In this study, the performance of the study system was assessed in five selected regions located across four different continents: Asia, Europe, America, and Oceania. Each of these regions was chosen due to its potential for harnessing geothermal energy. Here is a brief overview of the selected cities within these regions:

Aomori, Japan (Asia): Aomori is a significant city in Japan, situated in Aomori Prefecture. It is recognized for its substantial geothermal energy potential.

Grosseto, Italy (Europe): Grosseto is located in the Toscana region of Italy and is known for its high geothermal energy resources.

Lhasa, China (Asia): Lhasa serves as the capital of Tibet and is often referred to as the capital of Tibet province. This city is situated in the Asian continent.

Wellington, New Zealand (Oceania): Wellington, the capital of New Zealand, is positioned in the southwestern part of the North Island, between the Cook Strait and the Remutaka Range. It is known for having a significant geothermal energy potential.

San Diego, USA (America): San Diego is a coastal city in the United States of America, with access to various energy resources, including geothermal energy (see Fig. 18).

The study evaluated the geothermal system's performance in these diverse regions, taking into account their unique geographic and climatic characteristics. This investigation aimed to determine the suitability of these areas for the implementation of the geothermal system.

Fig. 19 displays the hourly variations in the average T_0 throughout the year for the selected study cities. The graph illustrates that the average T_0 in these cities fluctuates between −15 °C and 35 °C.

When comparing the average T_0 among the study cities, it's worth noting that Grosseto, Aomori, Wellington, San Diego, and Lhasa exhibit higher temperatures throughout the year. These variations in T_0 are essential considerations for assessing the feasibility and performance of the geothermal system in these regions, as they impact the potential for harnessing geothermal energy effectively.

In this study, the influence of varying T_0 in the selected cities on the performance of the system was thoroughly examined. The analysis aims to evaluate the power generated by the system, specifically during the peak hours of daily electricity consumption. The system has been designed to provide support during peak consumption periods in the respective regions, addressing the critical need for additional electricity during these high-demand periods.

6.1. Results of case study

Geothermal power generation systems are an environmentally friendly means of producing electricity, as they harness geothermal thermal energy without relying on fossil fuels. The study focused on assessing the system's electricity production in peak load conditions, comprising the combined power output of the organic Rankine cycles and the FC, as well as power generation without the FC, cooling, and hydrogen production.

The system integrates a FC unit to enhance its electrical generation capabilities. This FC relies on hydrogen, which is generated by the EPEM (Electrochemical Proton Exchange Membrane) unit within the geothermal system, resulting in a low environmental impact. A FC is akin to a battery, but it operates continuously as long as it is supplied with the requisite fuel (hydrogen) and oxidant (air). This approach provides a practical solution for peak electricity demands within the network.

As depicted in Fig. 20, the system's performance is illustrated in terms of hydrogen production across the study cities. The PEM Electrolyzer unit's power requirements are met by the electricity generated by the ORC. Thus, it's important to note that changes in the system's electricity production directly affect hydrogen production. The results indicate that increased T_0 lead to decreased hydrogen production, with the highest rates observed during the winter months, particularly in January and February. When comparing the cities, Lhasa in China

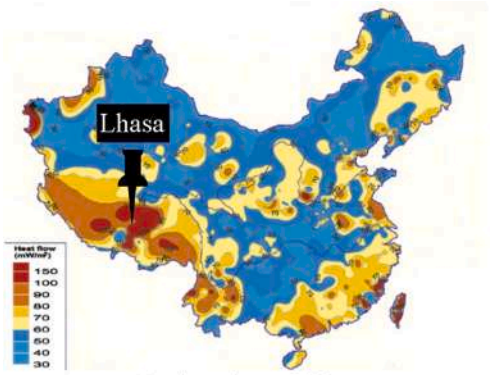

Geothermal map of China

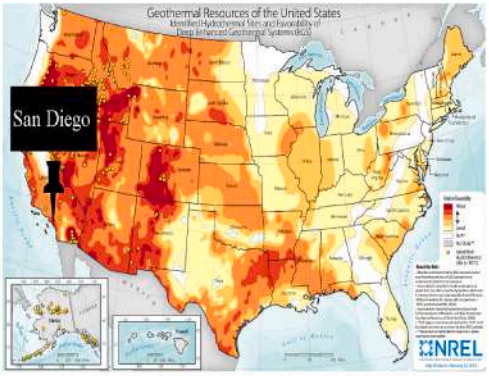

Geothermal map of United States of America

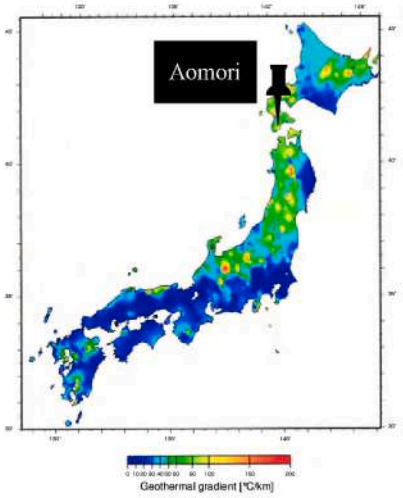

Geothermal map of Japan

Geothermal map of Italy

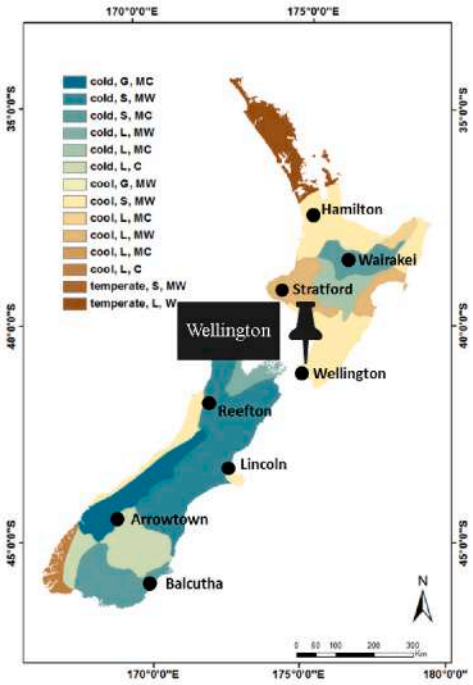

Geothermal map of New Zealand

Fig. 18. Geothermal map of the study areas.

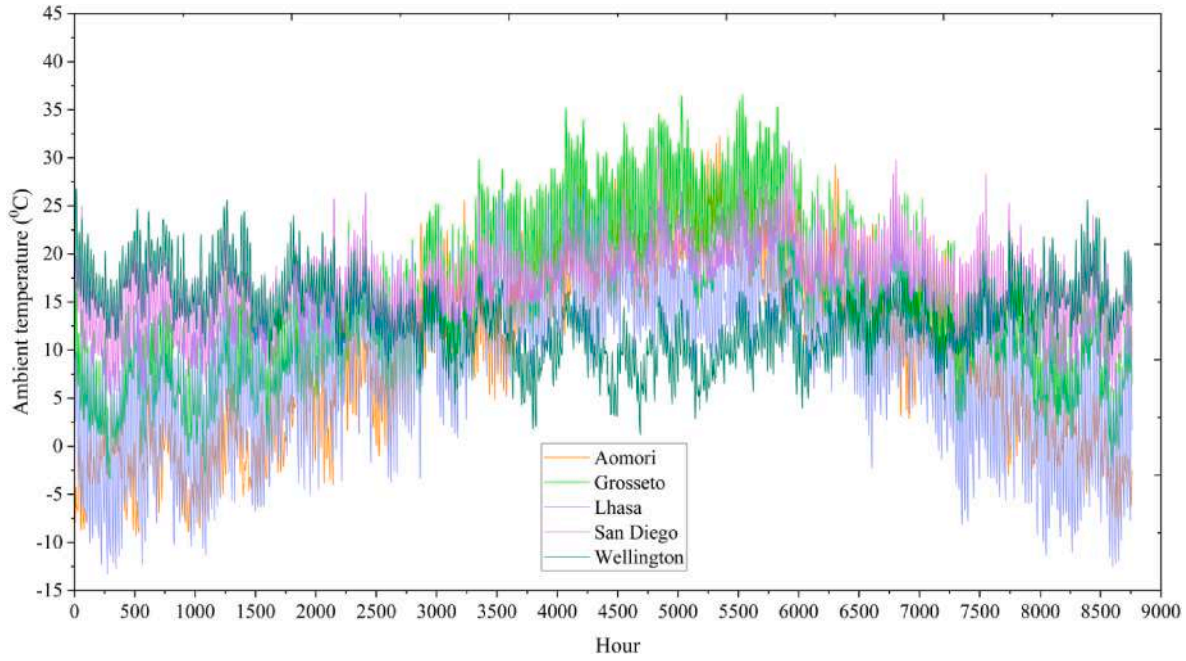

Fig. 19. Hourly variation of study cities ambient temperature per year.

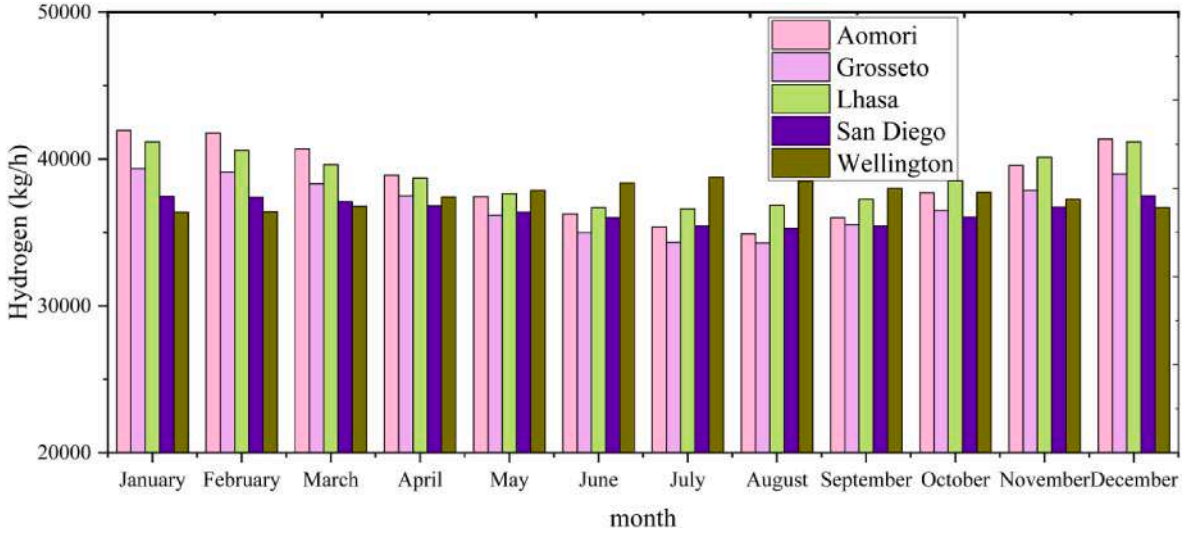

Fig. 20. Calculation of hydrogen produced in study cities.

exhibits the highest hydrogen production, while San Diego in the United States of America demonstrates the lowest hydrogen production.

The production power of the FC unit is calculated in Fig. 21. The results reveal a trend where elevated ambient temperatures are associated with reduced power production in the system's fuel cell unit. The highest power production rates are observed during the winter months, specifically in January and February. When comparing different cities, it is evident that Lhasa in China exhibits the highest production capacity for the fuel cell unit, whereas San Diego in the United States demonstrates the lowest power production rate for this component.

The performance of the system in generating electricity without using a fuel cell unit is checked in Fig. 22. The results indicate a noticeable inverse relationship between ambient temperature and the system's power output. Specifically, as ambient temperatures rise, the power generated by the system decreases. It is noteworthy that the peak period of power production occurs during the winter months of January and February.

Furthermore, a comparative analysis of various cities highlights distinctive power production patterns. The city of Lhasa in China stands out as the leader, exhibiting the highest power production rates. On the contrary, the city of San Diego in the United States of America demonstrates the lowest power production levels, marking a notable contrast in this regard.

In Fig. 23, we observe the evaluation of the entire system's power production while operating in conjunction with the FC unit. The utilization of a FC unit, especially during peak consumption periods in the cities under study, presents a viable solution for meeting energy demands, particularly during the high-load summer season.

Consistent with previous findings, these results also demonstrate a negative correlation between ambient temperature and power output. The system's power generation decreases as temperatures rise, underscoring the importance of climate conditions. The most significant power production rates occur during the winter months, specifically in January and February.

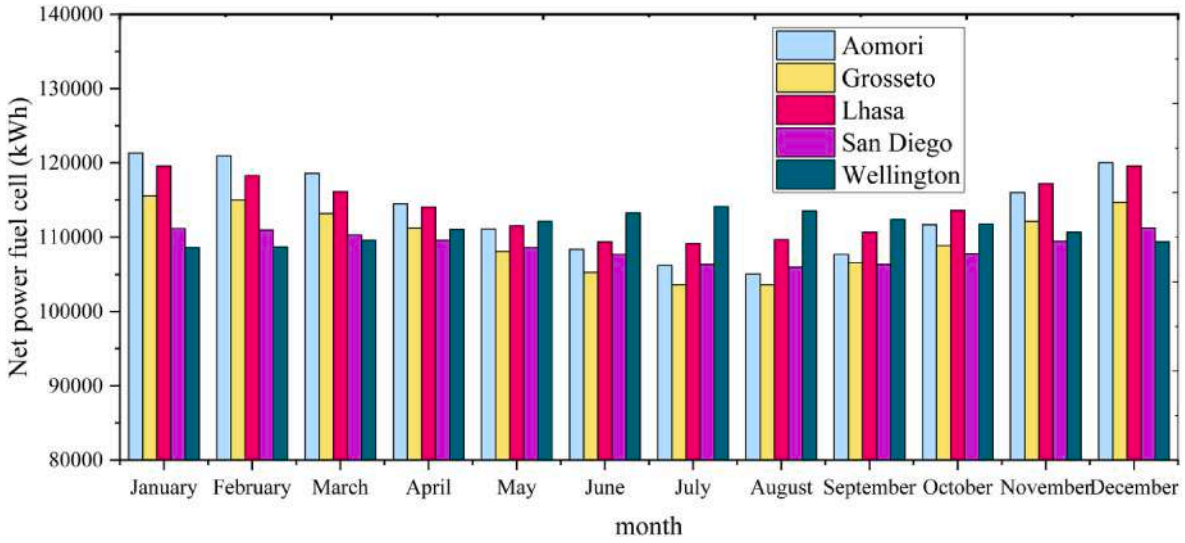

Fig. 21. Power generation calculation for study cities.

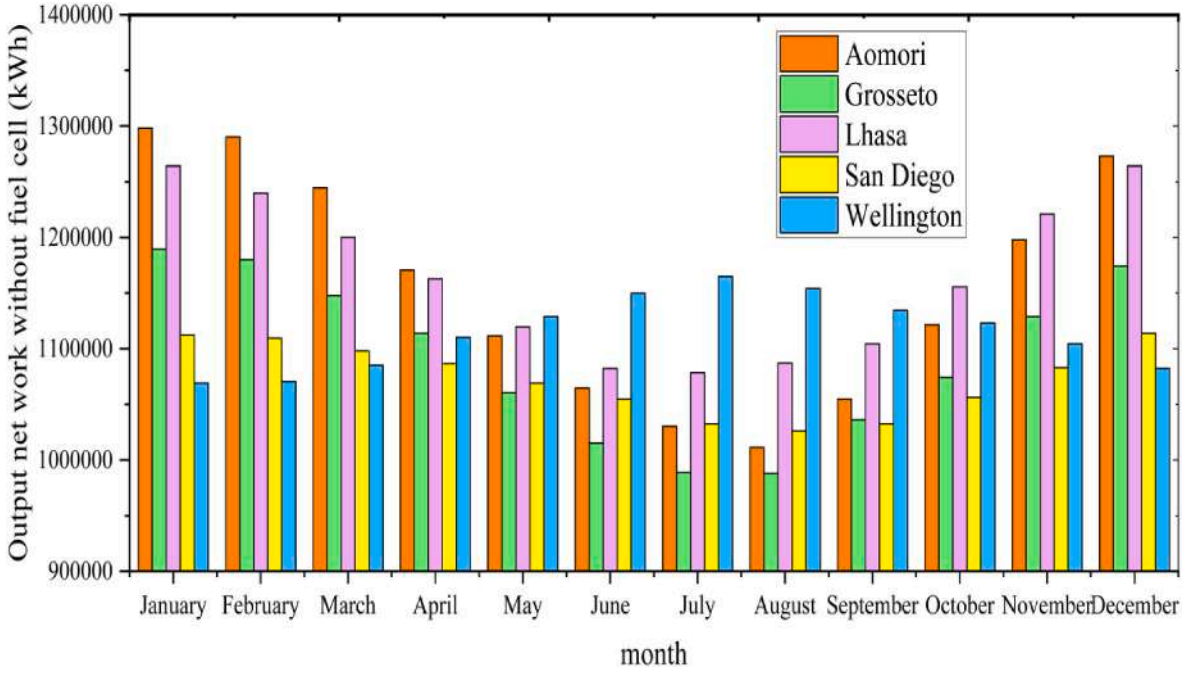

Fig. 22. Power generation without fuel cells calculation for study cities.

Additionally, when comparing power production across different cities, a distinct hierarchy emerges. Lhasa, China, maintains its position as the top performer, yielding the highest power production rates. In contrast, San Diego, United States, records the lowest power production levels, reaffirming the significance of location-specific factors in energy generation.

As depicted in Fig. 24, the evaluation of the system's cooling production is evident. The findings reveal a direct relationship between rising ambient temperatures and a reduction in the system's cooling efficiency. Interestingly, the system exhibits its highest cooling capacity during the winter months, specifically in January and February.

Moreover, when assessing the cooling production across various cities, a distinctive ranking emerges. Aomori city in Japan takes the lead, registering the highest cooling production rate. In contrast, Lhasa city in China shows the lowest cooling production rate, highlighting the significant variability in cooling capabilities across different locations.

Fig. 25 visually represents the monthly fluctuations in the system's exergy efficiency concerning shifts in ambient temperature. This graph underscores the detrimental effect of rising ambient temperatures on both power and hydrogen production. Consequently, it becomes evident that the exergy efficiency and power production rate share a direct relationship.

An important caveat to consider is that the unique geographical placement of the Oceania continent and the country of New Zealand results in a distinct performance pattern for the geothermal system when subjected to the weather conditions of Wellington city. This performance deviates significantly from the trends observed in the other cities studied.

7. Environmental analysis

The environmental analysis of the study system for the studied cities

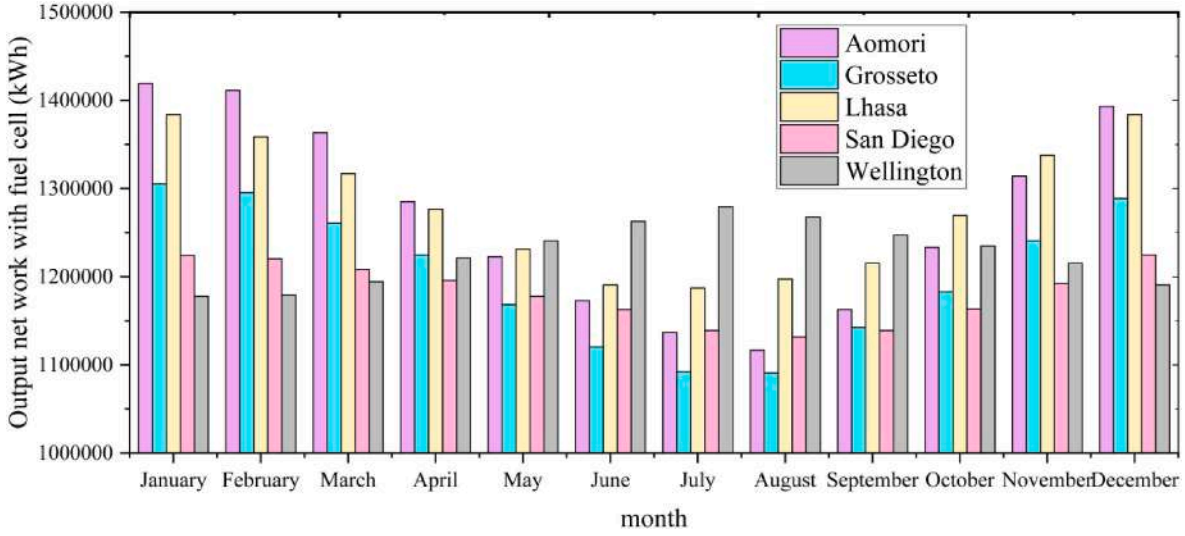

Fig. 23. Power generation by the system's fuel cell calculation for study cities.

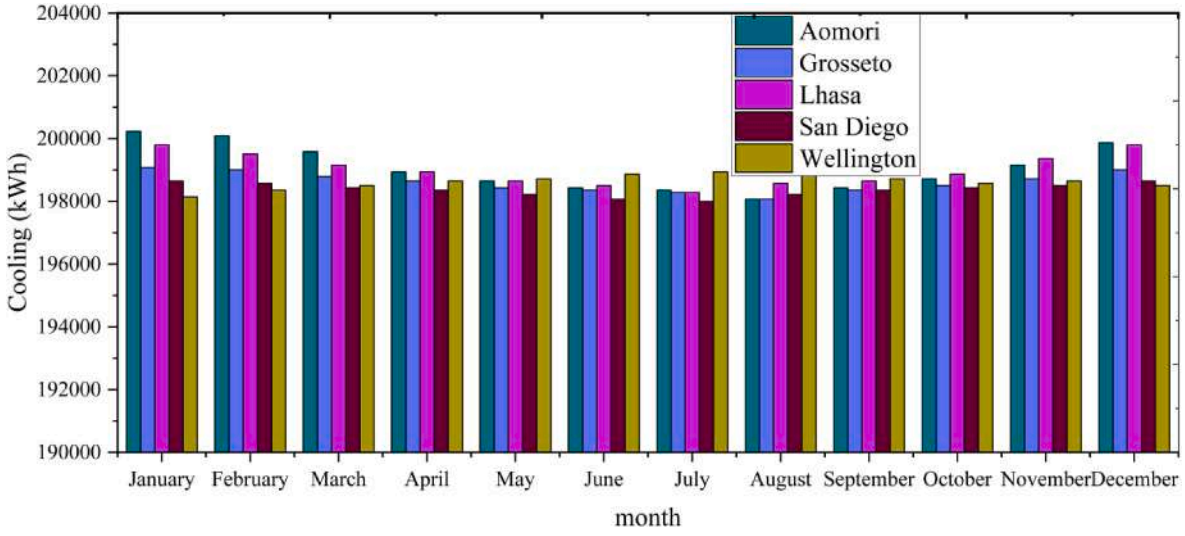

Fig. 24. Calculation of cooling rate produced for in study cities.

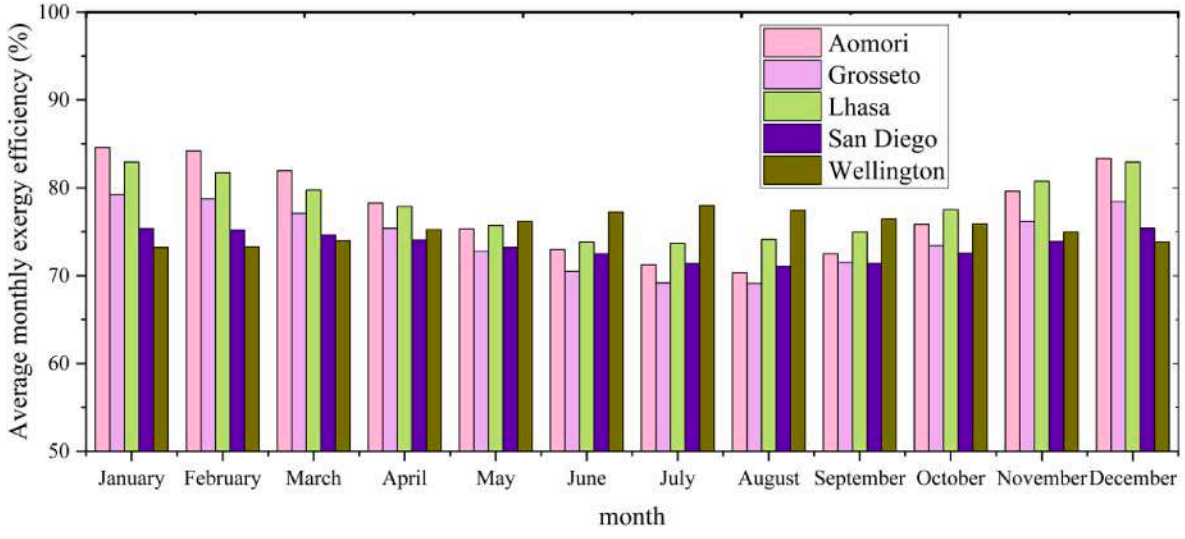

Fig. 25. Average monthly system exergy efficiency.

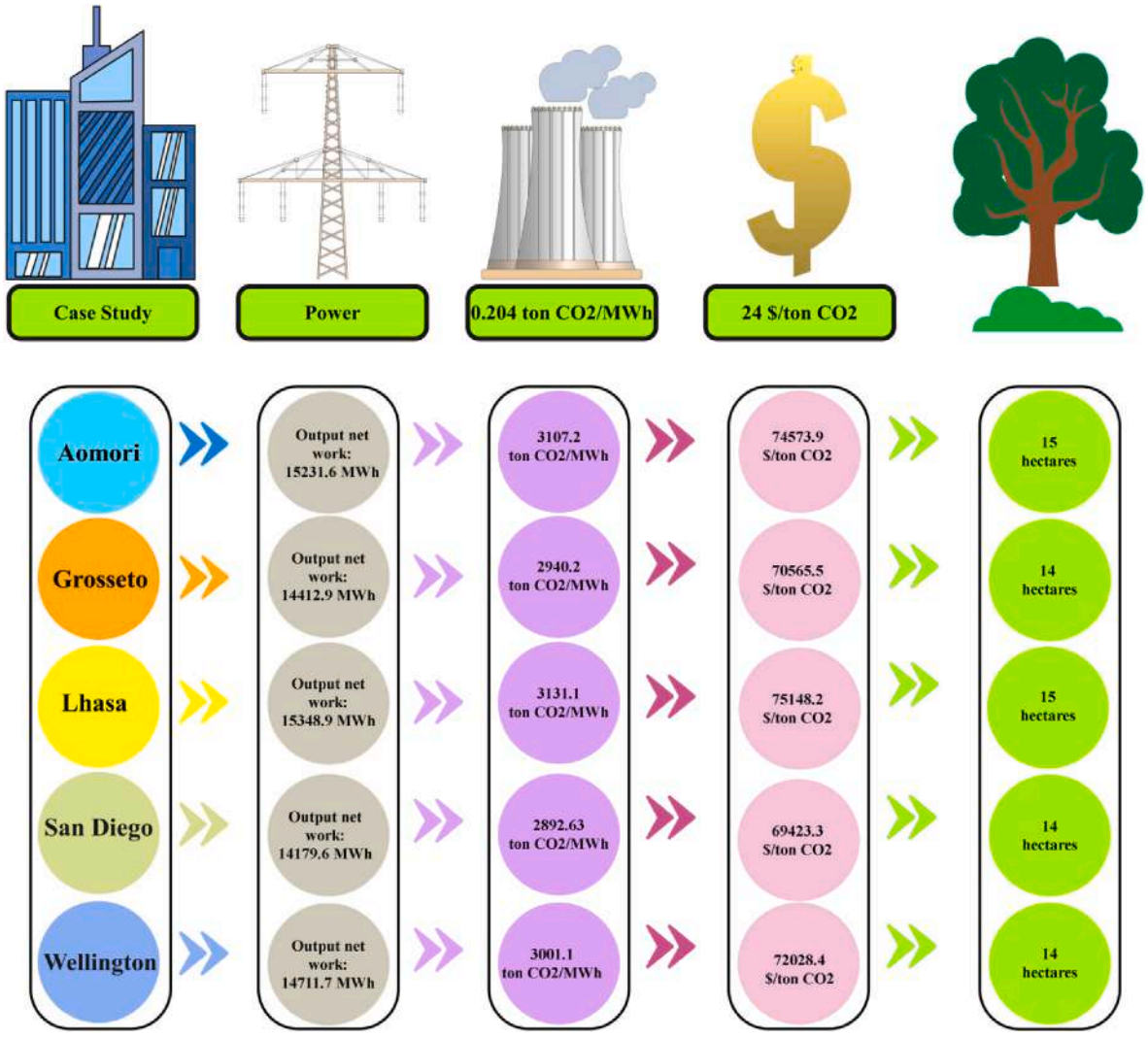

Fig. 26. Environmental analysis of the investigated system.

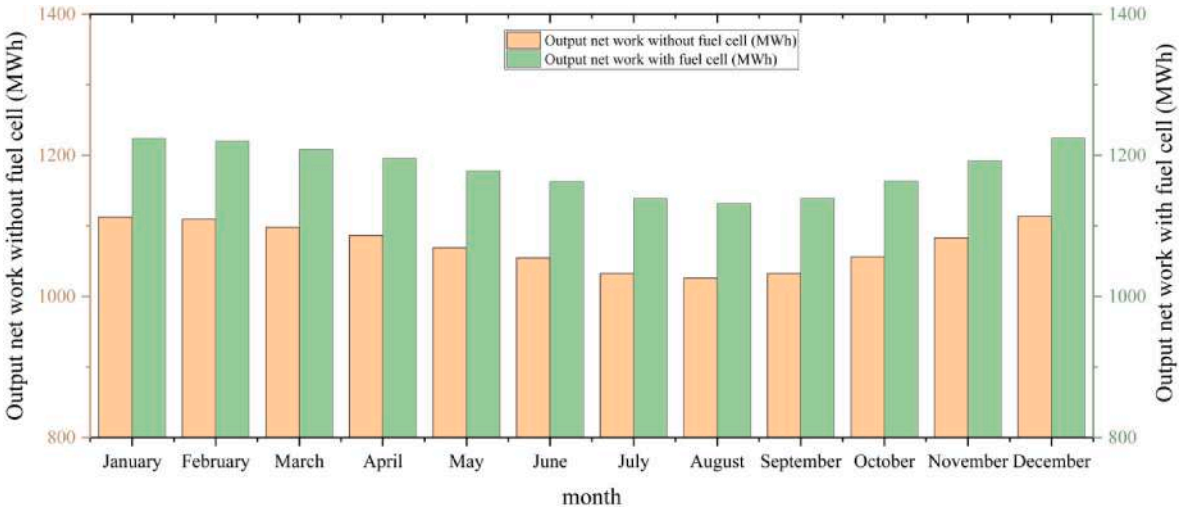

Fig. 27. Comparison of production power without fuel cell and with fuel cell of San Diego city.

Table 13
Calculate the amount of electricity needed for one person.

City	Power consumption for one person (kWh/per year)	Output Power (kwh/ peryear)	Number of people (−)	source
Aomori	*15231600*	*7150*	*2130*	*EIA (2019)*
Grosseto	*14412960*	*4928*	*2924*	*EIA (2019)*
Lhasa	*15348960*	*4617*	*3324*	*EIA (2019)*
San Diego	*14179680*	*12154*	*1166*	*EIA (2019)*
Wellington	*14711760*	*8372*	*1757*	*EIA (2019)*

Table 14
Characteristics of the walls and roof of the building.

	Thickness (m)	Conductivity Kj/hr.m.k	Capacity Kj/kg.k	Density Kg/m3
Plaster	*0.012*	*0.576*	*0.84*	*950*
Fiberglass	*0.066*	*0.144*	*0.84*	*12*
Wood siding	*0.009*	*0.504*	*0.9*	*530*
Plaster	*0.010*	*0.576*	*0.84*	*950*
Fiberglass	*0.112*	*0.144*	*0.84*	*12*
Roof desk	*0.019*	*0.504*	*0.9*	*530*

is reviewed in Fig. 26. This analysis is based on reference studies, which consider the various factors essential for evaluating pollution emissions, system costs, and the expansion of green spaces resulting from the implementation of the investigated system [42,43].

8. Analysis of consumption of residential building

Fig. 27 presents a comparative analysis of the power production of the system under two different scenarios: one without the use of the FC unit and the other with the inclusion of the FC unit. This analysis is specific to the city of San Diego, United States, as part of the current geothermal system research.

The findings clearly show that incorporating the fuel cell unit results in a notable increase in the system's power production. The use of a power-generating fuel cell unit during peak consumption periods in San Diego, particularly during the summer and winter seasons when heating and cooling systems are in high demand due to hot and cold weather conditions, emerges as an effective solution for meeting energy requirements.

8.1. Yearly electricity consumption for one person

In Table 13, the amount of electricity required for each person in the study cities has been calculated, and then the supply of energy needed by people by setting up the system in the study cities has been calculated (EIA [44]).

8.2. Annual power consumption of buildings

The envisioned building in San Diego is designed as a 4-story apartment complex, featuring one unit on each floor, resulting in a total of 4 individual units. It is assumed that each household within these units consists of 2 occupants. The area of each unit is 25 square meters, with each unit being treated as a distinct zone. In Table 14, you can find detailed information regarding the types of external walls and the roof characteristics of this apartment complex.

Fig. 28 illustrates the annual electricity consumption, measured in kilowatt-hours (kWh), for the specified apartment in the city of San Diego. This graph provides an overview of the electricity load consumed by the apartment over the course of a year.

Table 15 provides a detailed assessment of the system's performance in terms of energy production and its capacity to supply power to the apartment throughout the entire year. This table presents valuable

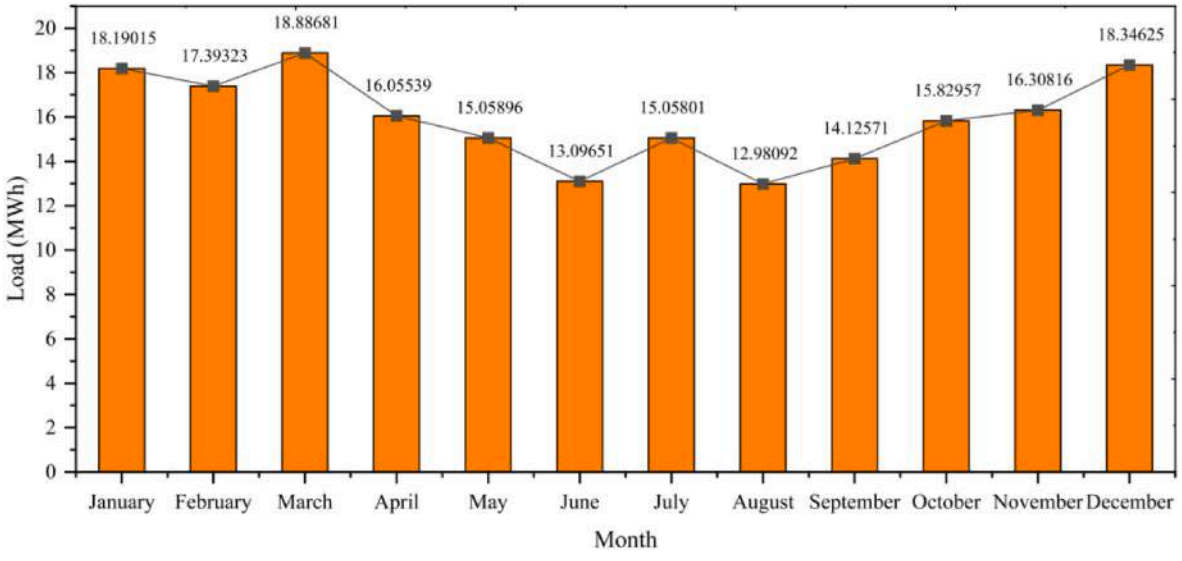

Fig. 28. Power load of the residential building.

Table 15
Supplied power demand of residential buildings.

City	Power generation (kwh/ peryear)	Electricity Demand (kwh/ peryear)	Power Export to Grid (kwh/ peryear)	Number of Buildings (−)	Number of Apartment Units (−)
San Diego	14179680	191330.9	13988349	74	296

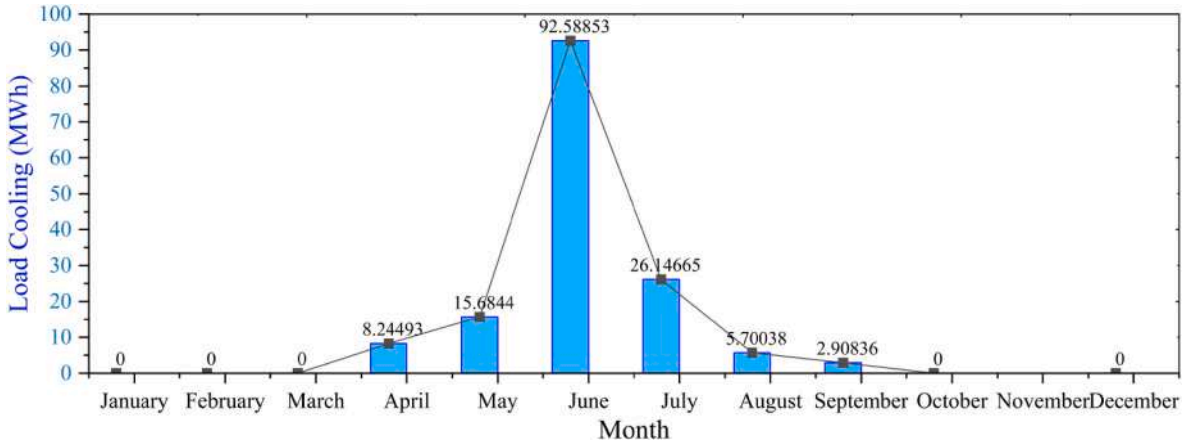

Fig. 29. Cooling load of the Building.

Table 16
Supply of cooling energy for residential units.

City	Cooling generation (kwh/peryear)	Cooling Demand (kwh/peryear)	Cooling Exports (kwh/peryear)	Number of Buildings (–)	Number of Apartment Units (–)
San Diego	2379672	151281	2229183	15	60

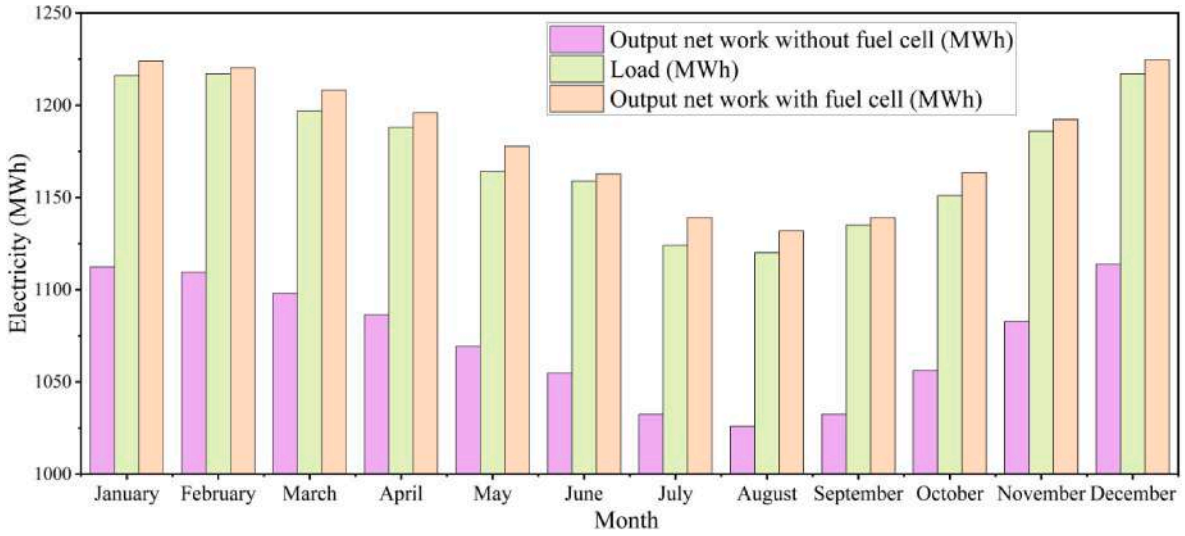

Fig. 30. Electricity for 74 buildings.

insights into the system's effectiveness in meeting the apartment's power needs over different seasons and under various conditions.

The suggested geothermal system's ability to produce cooling without the need for electricity consumption represents a notable advantage of the system. This feature is a significant strength, as it harnesses thermal energy from the ground to provide cooling, minimizing the reliance on external electricity sources and enhancing the system's overall efficiency.

8.3. The annual cooling rate of the residential complex

Fig. 29 visually represents the hourly cooling consumption of the specified apartment throughout the year in the city of San Diego. This graph offers a detailed view of the apartment's cooling needs over the course of each day, providing insights into how cooling requirements fluctuate with time.

Table 16 provides a comprehensive analysis of the system's performance concerning energy production and its effectiveness in delivering cooling to the apartment in the city of San Diego over the entire year. This table offers valuable insights into how the system performs in meeting the apartment's cooling requirements throughout the different seasons and under varying conditions.

The analysis revealed that the suggested geothermal system not only successfully met the cooling demands of the building but also had surplus cooling capacity that could be supplied to other residential buildings, generating revenue to cover maintenance costs. The system's utilization of thermal energy for cooling without the need for electricity consumption is a significant advantage. This not only ensures energy efficiency but also frees up more electricity for various residential and industrial applications, contributing to increased overall energy availability and utilization.

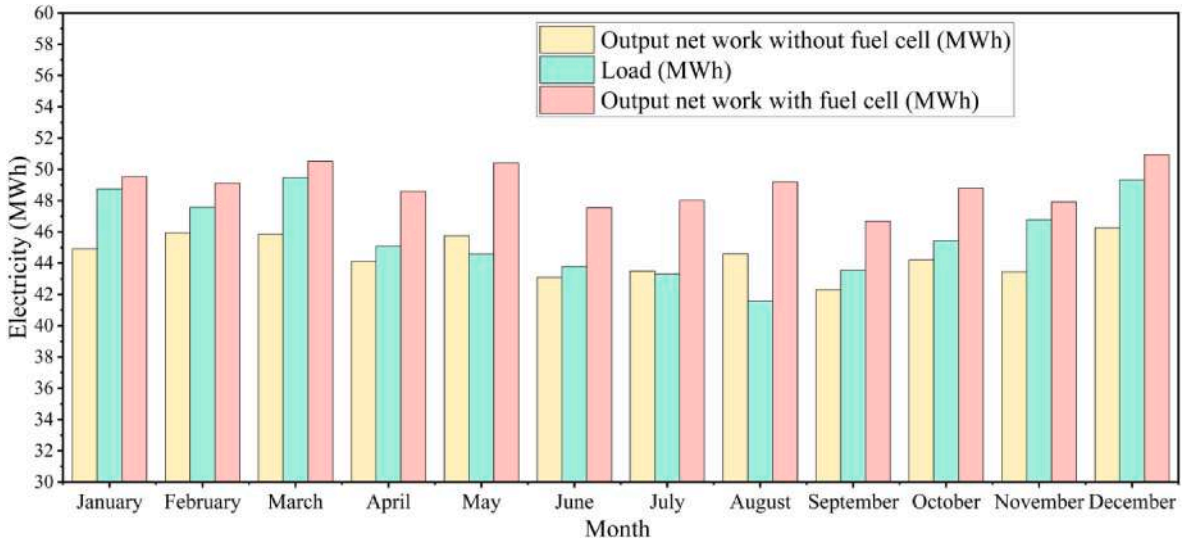

Fig. 31. Peak moving analysis.

8.4. The ability of the fuel cell to supply loads per year

In Fig. 30, an analysis of the electricity requirements for a residential complex consisting of 74 buildings, each with 4 units, in San Diego city is presented. This research incorporates the use of a FC as an energy storage device to fulfill the electricity needs of this residential complex.

The graph reveals the amount of electricity generated by the system without a FC, with production ranging from 500 MWh in August to 1100 MWh in December, as indicated by the blue line. Simultaneously, the electricity demand of the building complex is depicted in the green portion of the graph. The comparison between the green and orange graphs underscores that a FC is necessary in all months of the year to meet the complex's electricity requirements, highlighting the essential role of the FC in providing a consistent power supply.

8.5. Peak moving analysis

In this research, the utilization of a FC unit as an energy storage solution is crucial, particularly during peak consumption periods. Fig. 31 visually illustrates the rationale behind employing a fuel cell as a storage option during these peak times. The results in this figure have been specifically analyzed for 2 p.m. in a selected month of the year, which corresponds to a high-demand, peak consumption time. This underlines the significance of the FC's role in meeting the surges in electricity demand, ensuring a stable and reliable power supply.

9. Conclusion

The production of clean electrical energy during peak consumption periods is a pivotal innovation in this research. The suggested geothermal system is meticulously designed to cater to the escalating demand for electricity during peak consumption seasons. A key advantage of this system is its utilization of hydrogen fuel, renowned for its high efficiency, environmental cleanliness, and freedom from pollutants. The study focuses on addressing peak consumption challenges in urban areas and introduces a multi-objective model for optimizing a geothermal-based renewable energy system. This optimized system integrates various components, including single-effect absorption chiller units, PEMFC, EPEM, and two ORC units. A feasibility case study is conducted to assess the implementation of the geothermal system in diverse continents, including Asia, Oceania, Europe, and America, taking into account the influence of local weather conditions. The primary objective of this study system is to generate clean, carbon-free products with minimal environmental impact. System modeling is done using EES software, and optimization efforts are focused on increasing performance by considering three objective functions. Optimization is also done using the RSM. Additionally, the research explores the identification of the optimal organic fluids for use in organic Rankine cycles through six different scenarios, with the final selection being scenario NO. 3, incorporating R123 and R134a refrigerants. The results indicate achieve an impressive exergy efficiency rate of 81.816%, produce hydrogen at a rate of 25.119 kg/h, and operate at a cost rate of 15.967 $/h. Economic analysis highlights that the ORC 1 and 2 incur the highest system costs among the various components. The performance of the system is examined across five different cities, including Aomori, Grosseto, Lhasa, Wellington, and San Diego. The research concludes by assessing the capacity of the system to provide electricity, heating, and cooling for residential complexes in these study areas, underscoring its potential impact on meeting diverse energy needs in urban settings.

CRediT authorship contribution statement

Ehsanolah Assareh: Conceptualization, Data curation, Formal analysis, Funding acquisition, Investigation, Methodology, Project administration, Resources, Software, Supervision, Validation, Visualization, Writing – original draft, Writing – review & editing. **Parviz Ghafariasl:** Conceptualization, Formal analysis, Investigation, Visualization, Writing – original draft. **Siamak Hoseinzadeh:** Conceptualization, Data curation, Formal analysis, Funding acquisition, Investigation, Methodology, Project administration, Resources, Software, Supervision, Validation, Visualization, Writing – original draft, Writing – review & editing. **Neha Agarwal:** Conceptualization, Data curation, Formal analysis, Investigation, Methodology, Software, Validation, Visualization, Writing – original draft. **Moonyong Lee:** Conceptualization, Funding acquisition, Methodology, Project administration, Resources, Supervision, Visualization, Writing – review & editing. **Davide Astiaso Garcia:** Conceptualization, Funding acquisition, Methodology, Resources, Supervision, Writing – review & editing.

Declaration of competing interest

The authors declare that they have no known competing financial interests or personal relationships that could have appeared to influence the work reported in this paper.

Acknowledgment

This work was supported by the National Research Foundation of Korea (NRF) grant funded by the Korea government (MSIT) (2021R1A2C1092152).

Appendix A. Supplementary data

Supplementary data to this article can be found online at https://doi.org/10.1016/j.ijhydene.2024.08.080.

References

[1] Batista NE, et al. Optimizing methodologies of hybrid renewable energy systems powered reverse osmosis plants. Renew Sustain Energy Rev 2023;182:113377.
[2] Axelsson G. 7.01 - introduction to volume on geothermal energy. Comprehensive renewable energy. second ed. Oxford: Elsevier; 2022. p. 1–2. T. M. Letcher.
[3] Sigfusson TI. 7.01 - geothermal energy – introduction. Comprehensive renewable energy. A. Sayigh. Oxford. Elsevier; 2012. p. 1–2.
[4] Giambastiani BMS, et al. Energy performance strategies for the large scale introduction of geothermal energy in residential and industrial buildings: the GEO. POWER project. Energy Pol 2014;65:315–22.
[5] Xie Y, et al. Flash evaporation strategy of organic Rankine cycle for geothermal power performance enhancement: a case study. Renew Energy 2023;212:57–69.
[6] Singh A, et al. Comparing solar collector efficiency with different organic fluids. Mater Today Proc 2023.
[7] Zhang X, Li Y. An examination of super dry working fluids used in regenerative organic Rankine cycles. Energy 2023;263:125931.
[8] Li T, et al. Geothermal power generation improvement of organic Rankine flash cycle using exergy, advanced exergy and exergoeconomic analyses. Appl Therm Eng 2023;223:120032.
[9] Tao J, et al. Pakistan's electrical energy crises, a way forward towards 50% of sustain clean and green electricity generation. Energy Strategy Rev 2022;40:100813.
[10] Scott K. 4.01 - introduction to hydrogen, electrolyzers and fuel cells science and technology. Comprehensive renewable energy. second ed. Oxford: Elsevier; 2022. p. 1–28. T. M. Letcher.
[11] Rahimnejad M. Chapter 1 - introduction to biological fuel cell technology. Biological Fuel Cells. M. Rahimnejad, Elsevier 2023:3–28.
[12] Sun E, et al. Proposal and application of supercritical steam Rankine cycle using supercritical reheating regeneration process and its comparison between S-CO2 Brayton cycle. Energy Convers Manag 2023;280:116798.
[13] Kang L, et al. Research on energy management of integrated energy system coupled with organic Rankine cycle and power to gas. Energy Convers Manag 2023;287:117117.
[14] Akrami E, et al. Exergy and exergoeconomic assessment of hydrogen and cooling production from concentrated PVT equipped with PEM electrolyzer and LiBr-H2O absorption chiller. Int J Hydrogen Energy 2018;43(2):622–33.
[15] Martinez Lopez VA, et al. Dynamic operation of water electrolyzers: a review for applications in photovoltaic systems integration. Renew Sustain Energy Rev 2023;182:113407.
[16] Cao L, Lou J, Wang J, Dai Y. Exergy analysis and optimization of a combined cooling and power system driven by geothermal energy for ice-making and hydrogen production. Energy Convers Manag 2018;174:886–96.
[17] Alirahmi SM, Assareh E. Energy, exergy, and exergoeconomics (3E) analysis and multi-objective optimization of a multi generation energy system for day and night time power generation-Case study: dezful city. Int J Hydrogen Energy 2020;45(56):31555–73.
[18] Ren F, Wang J, Zhu S, Chen Y. Multi-objective optimization of combined cooling, heating and power system integrated with solar and geothermal energies. Energy Convers Manag 2019;197:111866.
[19] Briolaa S, Gabbrielli R, Bischi A. Off-design performance analysis of a novel hybrid binary geothermalbiomasspower plant in extreme environmental conditions. Energy Convers Manag 2019;195:210–25.
[20] Li H, et al. Study on the biomass-based SOFC and ground source heat pump coupling cogeneration system. Appl Therm Eng 2020;165:114527.
[21] Atiz A, et al. Investigation energy, exergy and electricity production performance of an integrated system based on a low-temperature geothermal resource and solar energy. Energy Convers Manag 2019;195:798–809.
[22] Xie J, Wang J. Compatibility investigation and techno-economic performance optimization of whole geothermal power generation system. Appl Energy 2022;328:120165.
[23] Zhong C, et al. The feasibility of clean power generation from a novel dual-vertical-well enhanced geothermal system (EGS): a case study in the Gonghe Basin, China. J Clean Prod 2022;344:131109.
[24] Mardan Dezfouli AH, et al. Energy, exergy, and exergoeconomic analysis and multi-objective optimization of a novel geothermal driven power generation system of combined transcritical CO2 and C5H12 ORCs coupled with LNG stream injection. Energy 2023;262:125316.
[25] Seiiedhoseiny M, et al. Exergoeconomic analysis and optimization of a high-efficient multi-generation system powered by Sabalan (Savalan) geothermal power plant including branched GAX cycle and electrolyzer unit. Energy Convers Manag 2022;268:115996.
[26] Pan J, et al. Energy, exergy and economic analysis of different integrated systems for power generation using LNG cold energy and geothermal energy. Renew Energy 2023;202:1054–70.
[27] Jiansheng W, et al. Numerical investigation on power generation performance of enhanced geothermal system with horizontal well. Appl Energy 2022;325:119865.
[28] Soltani M, Nabat MH, Razmi AR, Dusseault MB, Nathwani J. A comparative study between ORC and Kalina based waste heat recovery cycles applied to a green compressed air energy storage (CAES) system. Energy Convers Manag 2020;222:113203. https://doi.org/10.1016/j.enconman.2020.113203.
[29] Razmi A, Soltani M, Tayefeh M, Torabi M, Dusseault MB. Thermodynamic analysis of compressed air energy storage (CAES) hybridized with a multi-effect desalination (MED) system. Energy Convers Manag 2019;199:112047. https://doi.org/10.1016/j.enconman.2019.112047.
[30] Dincer, Rosen MA, Ahmadi P. Optimization of energy systems. Chichester, UK: John Wiley & Sons, Ltd; 2017.
[31] Razmi AR, Janbaz M. Exergoeconomic assessment with reliability consideration of a green cogeneration system based on compressed air energy storage (CAES). Energy Convers Manag 2020;204(October):112320. Jan. 2020.
[32] Wang C, Jin H, Peng P, Chen J. Thermodynamics and LCA analysis of biomass supercritical water gasification system using external recycle of liquid residual. Renew Energy 2019;141:1117–26. https://doi.org/10.1016/j.renene.2019.03.129.
[33] Carmo M, Fritz DL, Mergel J, Stolten D. A comprehensive review on PEM water electrolysis. Int J Hydrogen Energy 2013;38:4901–34. https://doi.org/10.1016/j.ijhydene.2013.01.151.
[34] Akrami E, Nemati A, Nami H, Ranjbar F. Exergy and exergoeconomic assessment of hydrogen and cooling production from concentrated PVT equipped with PEM electrolyzer and LiBr-H2O absorption chiller. Int J Hydrogen Energy 2018;43:622–33. https://doi.org/10.1016/j.ijhydene.2017.11.007.
[35] Changizian S, Ahmadi P, Raeesi M, Javani N. Performance optimization of hybrid hydrogen fuel cell-electric vehicles in real driving cycles. Int J Hydrogen Energy 2020:1–18. https://doi.org/10.1016/j.ijhydene.2020.01.015.
[36] Alirahmi SM, Rostami M, Farajollahi AH. Multi-criteria design optimization and thermodynamic analysis of a novel multi-generation energy system for hydrogen, cooling, heating, power, and freshwater. Int J Hydrogen Energy 2020;45:15047–62. https://doi.org/10.1016/j.ijhydene.2020.03.235.
[37] Wang Y, et al. BMW-TOPSIS: a generalized TOPSIS model based on three-way decision. Inf Sci 2022;607:799–818.
[38] Zhang K, Dai J. A novel TOPSIS method with decision-theoretic rough fuzzy sets. Inf Sci 2022;608:1221–44.
[39] Allaix DL, Carbone VI. An improvement of the response surface method. Struct Saf 2011;33(2):165–72.
[40] Li D-Q, et al. Response surface methods for slope reliability analysis: review and comparison. Eng Geol 2016;203:3–14.
[41] Ioroi T, Yasuda K, Siroma Z, Fujiwara N, Miyazaki Y. Thin film electrocatalyst layer for unitized regenerative polymer electrolyte fuel cells. J Power Sources 2002;112:583–7.
[42] Kroegera T, Escobedob FJ, Hernandezc JH, Varelab S, Delphinb S, Fishera JRB, Waldrond J. Reforestation as a novel abatement and compliance measure for ground-level ozone. 2014. p. 111. https://doi.org/10.1073/pnas.1409785111. 40.
[43] https://www.gov.uk/government/publications/greenhouse-gas-reporting-conversion-factors- updated 28 July 2020.
[44] https://www.eia.gov/.S.EnergyInformationAdministration1000IndependenceAve., SW Washington, DC 20585/electricity consumption.